SINGLE MOLECULE TRACKING STUDIES OF THE NANOSCALE PROPERTIES OF SOL-GEL-DERIVED SILICA THIN FILM GRADIENTS

by

CHENCHEN CUI

B.E., Nanjing University of Science and Technology, 2005
M.E., Nanjing University of Science and Technology, 2007

A THESIS

Submitted in partial fulfillment of the requirements for the degree

MASTER OF SCIENCE

Department of Chemistry
College of Arts and Sciences

KANSAS STATE UNIVERSITY
Manhattan, Kansas

2011

Approved by:

Major Professor
Daniel. A. Higgins

Copyright

Abstract

Single molecule tracking (SMT) measurements have been applied to the study of molecular mobility in sol-gel-derived silica gradient films in this thesis. Such gradient films have broad potential applications in controlled adhesion and transport of cells, vesicles and polymers; separation of complex chemical mixtures and in the development of new catalysts. Silica films were prepared by "infusion-withdrawal dip-coating".[1] In this method, a suitable substrate is slowly withdrawn from a silica sol of time varying composition. The deposition reservoir is initially filled with a sol derived from one silica precursor (tetramethoxysilane). A second sol, prepared from a different precursor (methyltrimethoxysilane), is then infused into the deposition reservoir, as the mixed sol is withdrawn. Films thus prepared were initially characterized by bulk fluorescence spectroscopy, infrared (IR) microscopy, contact angle goniometry, spectroscopic ellipsometry and surface profilometry. The fluorescence, IR and contact angle data all demonstrate the presence of a gradient in the methyl content of the silica film. The primary objective of the work performed under this thesis was to investigate the diffusion of Nile Red molecules in and on these films, as a function of position along the gradient, by SMT methods. Histograms of the mean-square displacement of the molecules depict the presence of at least two distinct populations: one incorporating fixed (entrapped or adsorbed) molecules and the other clearly reflecting the presence of mobile molecules. The latter population was observed to vary along the gradient dimension and also changed as the films aged over the course of five days. Molecular mobility is attributed to the presence of liquid-like silica oligomers in the films. Spatial variations in the observed mobility are tentatively assigned to variations in oligomer viscosity along the gradient. Film viscosity also changes as the polymerization of the oligomers continues during film aging.

Table of Contents

List of Figures

Acknowledgements

I would like to give my sincere gratitude to my advisor Dr. Daniel A. Higgins. I am hard pressed to imagine a better role model, in terms of his inimitable enthusiasm, inspiration, encouragement, guidance and instruction. He was always supportive throughout my pursuit of the Master's Degree, which enabled me to develop a better understanding of the study. I feel extraordinarily lucky to have had the opportunity to work with and learn from him.

I would also like to thank Dr. Maryanne M. Collinson for giving me insightful advice on my research, and to Alec Kirkeminde and Balamurali Kannan for working together with me on the sol-gel project. Thank to all the Higgins' group members that passed through while I was here: Dr. Fangmao Ye, Dr. Jeff Lange, Dr. Thomas Everett, and Seokchan Park. They were always sharing their research skills and were very helpful in lab.

I would also like to thank all of my committee members, Dr. Kenneth Klabunde, Dr. Christopher Culberson, and others in the Kansas State University Chemistry Department, especially Jim Hodgson for making the glass cells for my research, which I broke time to time.

Finally, I would like to show my appreciation for my family and friends for all their love and support. It is them that have kept me going through all the difficulties and not being lost on the way.

Dedication

This work is dedicated to my parents.

Chapter 1 - Introduction

Sol-gel-derived silica thin films represent a technologically important class of materials having a variety of applications in chemical analysis, such as in chromatographic separations, in catalysis, in fuel cells, and as supports for optical sensors.[2-8] The successful implementation of silica materials in these applications relies on efficient transport and partitioning of molecules within silica films and on their surfaces. For example, the response of a sensor depends on how quickly analyte molecules can diffuse into the material matrix to immobilized reagent molecules that produce the sensor response. Catalyst poisoning or peak tailing in separations would be caused by molecules that become permanently trapped in the silica matrix. So the film properties and the interaction between guest molecules and the silica films need to be understood.

For a variety of applications of silica thin films, such as absorbent/adsorbent layers for use in chemical or biological sensors,[9] materials for combinatorial catalysis,[10] and stationary phases for chemical separations,[11] information on film structure, film heterogeneity, and guest molecule mobility in/on the film is important, but is difficult to obtain from traditional analysis methods. Single molecule studies can be used to evaluate the microscopic structure of such materials, and single molecule tracking (SMT) can be used to investigate the dynamic motion of guest molecules in the nanoscale structure at the same time. By detection of molecular movement and analysis of molecule trajectories, the interactions between guest molecules and such materials can be interpreted, and the local silica properties can be studied. Since single molecule methods provide useful means for understanding molecular movement in thin film materials and film nanoscale properties, they were applied to sol-gel-derived silica thin films in this research.

1.1 Sol-gel derived silica thin film gradients

Silica materials incorporating inorganic/organic functional groups can be designed to have a broad range of chemical and physical properties. Such materials have been explored previously for use in ion exchange methods,[12] chemical sensing,[13-15] catalysis[16,17] and chemical separations.[18-20] The sol-gel process[2,21,22] represents an important and convenient route to the

preparation of a virtually unlimited range of silica materials. Although simple "inorganic" silica materials can be prepared by the hydrolysis and condensation of precursors such as tetramethoxysilane (TMOS),[2,21,22] more complex organic-inorganic hybrid materials can be achieved by blending TMOS-based sols with those derived from any of a wide variety of commercially available organoalkoxysilanes having the formula $RSi(OMe)_3$, where R represents a nonhydrolyzable organic substituent.[3,23,24]

The complete optimization of silica film properties for use in a particular application would require preparation and characterization of a large variety of films from sols of varying composition (i.e., using organosilanes with different R groups), inorganic/organic precursor mole ratio, sol pH, etc. Such studies would be extremely time consuming, and ultimately only a very narrow range of materials would be found useful for the intended application. A much more efficient route for materials optimization is through the preparation of continuously graded films, whereby the composition of the sol employed is gradually varied during production of a single film. Indeed, such gradient materials have long been investigated for use in "combinatorial" (or high-throughput screening) studies of other inorganic, organic and polymeric materials.[25,26]

Thin films can be prepared by a variety of methods, including spin-coating and dip-coating of the sol onto a suitable substrate.[21] In this thesis, an "infusion-withdrawal dip-coating" process is employed for the preparation of silica thin film gradients. Briefly, the silica thin film gradient is deposited on the substrate in a reservoir filled with a sol of time varying composition obtained by slowly mixing two different sols together. Aside from this recent work done by our group, only a single prior publication describing thickness gradients prepared by the sol-gel process appears in the literature.[27] While surface gradients obtained via the grafting of reactive chlorosilanes onto OH-terminated substrates have been widely reported,[28-34] the exploration of bulk inorganic/organic composite silica materials has not. Considering the potential of organically-modified silica films having a virtually unlimited range of properties, the preparation and study of graded materials by the sol-gel process is further needed.

1.2 Why single molecule methods?

Complete optimization of sol-gel derived silica materials for a variety of applications relies on efficient transport of molecules within the materials structure. Information on the diffusion process of guest molecules is indispensable to the elucidation of the chemical nature

and functionality of silica materials. A guest molecule's movement within the silica framework and its interactions with material surfaces is inherently dependent upon the nature of the local environment. While a large number of bulk spectroscopic[35-38] and electrochemical[39-43] studies of sol-gel-derived silica materials have been reported in the literature, the results of these studies yield, primarily, information on the average materials properties and average behavior of guest molecules. The extensive averaging that occurs in these experiments masks important information on nanoscale (and larger) variations in materials properties. If the behavior of single guest molecules can be studied instead, the heterogeneity of the film structure can be much better understood. This represents the primary motivation for single molecule research: to uncover the presence of and better understand the impacts of sample heterogeneity. Currently, single molecule methods are the best way of representing local chemical or physical material structure within thin films.

A simple illustration of the differences between bulk and single molecule studies is shown in Figure 1-1. This figure shows a simulated bulk fluorescence spectrum in black. The peak position of the spectrum is governed by the electronic properties of the fluorophore, namely the energy gap between its excited and ground electronic states. However, in heterogeneous materials, interesting information about the material in which the fluorophore is entrapped is contained in the peak width. The bulk spectrum is actually a sum of signals from many different (narrower) fluorescence spectra from single molecules in different chemical environments. Simulated single molecule spectra are depicted in Figure 1-1 by the colored spectra. Shifts in the single molecule spectra between the individual environments can arise for a number of different reasons. These include polarity, porosity, ionic site density, thickness, molecular weight, etc.[44-47] By recording only the bulk spectrum, much of the information on materials heterogeneity that is contained in the individual single molecule spectra is lost.

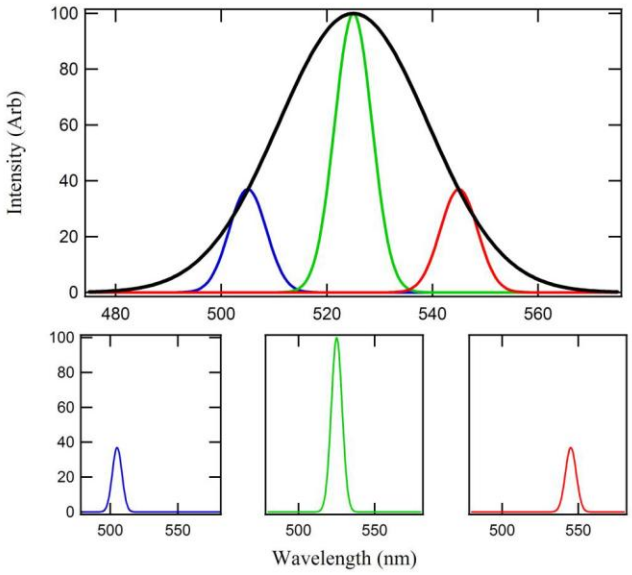

Figure 1-1. A simulated fluorescence spectrum, bulk fluorescence spectrum in black, while colored spectra correspond to identical single molecules in slightly different chemical environments.

By studying single molecule behaviors, which removes the usual ensemble averaging, information pertaining to the nanoscale materials environment and film heterogeneity can be obtained. Practically, the single molecule acts as a local reporter of its "nanoenvironment", it indicates the presence of local functional groups, surface properties, pore size, and matrix mobility, polarity and acidity. [1,44-54]

1.3 Single molecule tracking

In 1990 Michel Orrit and Jacky Bernard were able to show the detection of single molecules by fluorescence excitation for the first time.[55] Since then, single molecule fluorescence spectroscopy has become an essential tool for understanding single molecule behavior. One of the most important behaviors of an individual molecule is the molecule movement itself. In structured materials, molecules do not always move by Brownian motion, so by tracking the molecules, and studying lateral motion, angular motion, mobile and immobile populations, and diffusion coefficients, the local heterogeneities in material structure and properties can be explored. Single-molecule fluorescence imaging and single molecule tracking has become an independent discipline capable of solving problems by investigation of (or related to) molecular movement.

1.3.1 Single molecule tracking techniques

Single molecule techniques for studying molecular motions include fluorescence correlation spectroscopy (FCS) by confocal methods, and single molecule tracking by wide-field microscopy.[1,56] FCS and wide-field methods have their own advantages and disadvantages.

1.3.1.2 Fluorescence correlation spectroscopy (FCS) by confocal methods

Fluorescence correlation spectroscopy (FCS), invented in 1974,[57] is a technique in which a diffraction-limited laser beam, is focused into a sample using a high numerical aperture objective. The sample contains diffusing fluorophores at a low concentration (nM). The fluorescent species diffuse in and out of the observation volume, causing fluctuations in the fluorescence signal. The signal obtained is measured by a photo-detector. A diagram of an FCS experiment is shown in Figure 1-2.

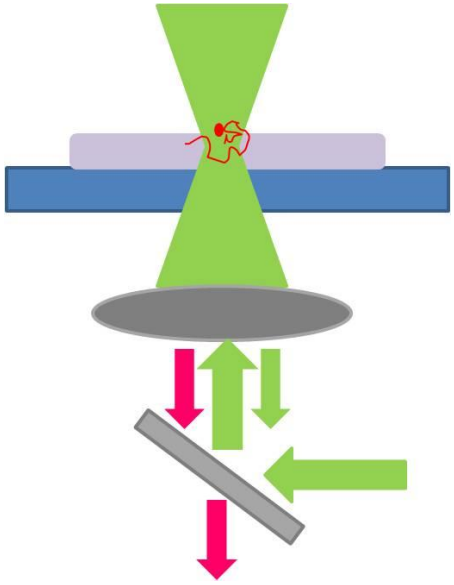

Figure 1-2. A diagram of an FCS experiment.

FCS data are obtained by recording fluorescence from a single point as single molecules wander through the excitation volume. Since the method is observing a small number of molecules in a very tiny spot, obtaining good data on the distribution of materials properties requires long observation periods, and access to spatial information is difficult.

1.3.1.3 Wide-field fluorescence microscopy

A typical diagram of the fluorescence microscope used in wide-field experiments[58] is shown in Figure 1-3. Laser light is reflected from a dichroic beamsplitter and is focused into the

back aperture of the objective. Then dye molecules in the sample are excited by the laser light, and emit fluorescence. Fluorescence from the sample is collected in reflection and is separated from the excitation light by passage back through the dichroic beamsplitter. A very sensitive electron-multiplying charge-coupled device (CCD) camera is used as the detector.[1]

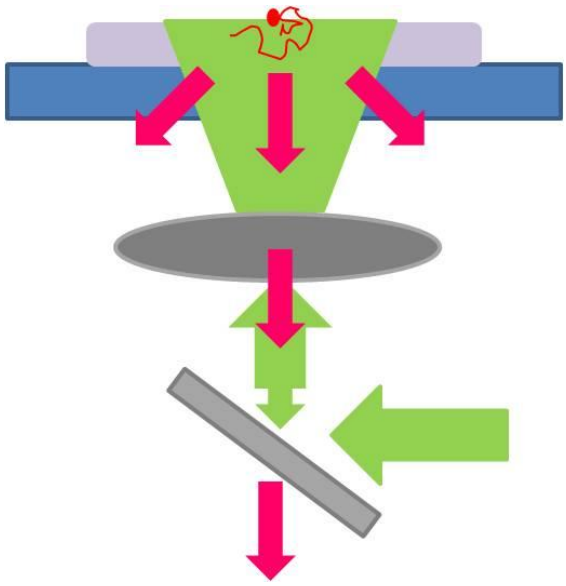

Figure 1-3. A diagram of a wide-field microscopy experiment.

A primary advantage of wide-field fluorescence microscopy is that it allows for imaging and recording the actual path (or trajectory) of several hundred molecules in parallel, under identical conditions, in a real image sequence. By taking a series of "molecule images" and following the actual path and time dependent motions of a molecule, the exact mode and dimension of molecular motion can be determined. This data can be used for tracking molecules and evaluating the microscopic structure of bio-related and technological materials and investigating the dynamic motion of molecules in nanoscale structures.[59]

1.3.1.4 Single molecule detection

The "single molecule images" on the camera can be very well approximated as a Gaussian spot. In reality the "image" of a molecule represents an image of the laser spot rather than the molecule. By tracking mobile spots in a series of images, the diffusion coefficients of the molecules can be determined. Some criteria that need to be fulfilled in the image: the S/N should be sufficient for the spots to be detected, the size of the spot should be diffraction-limited, and the molecule should be present in several consecutive frames. The position of the molecules

can even be determined to subpixel resolution, depending on the signal-to-noise ratio, by fitting their fluorescence intensity distributions to a Gaussian function.[60]

1.3.1.5 Single molecule tracking analysis

Diffusion through silicate films

It is important to understand how quickly molecules diffuse though silica materials, because the rate of diffusion can affect their applications, such as in chromatographic separations, in optical sensors, and in catalyst supports. For example, catalytic rates depend on how quickly reagent molecules can diffuse into the silica matrix to the immobilized catalyst sites, and the cycle time also depends on how quickly the products can diffuse out of the structure. Several methods have been used for studying molecular diffusion in silica materials, such as electrochemistry[61,62] and total internal reflectance Fourier transform infrared spectroscopy[58]. These methods probe the diffusion of molecules over a large area of the sample, and yield ensemble averaged data. None of them investigates the differences in the rates of transport that might arise from the heterogeneity of the materials, which is important because these materials can be structurally and chemically heterogeneous. Such heterogeneity can lead to trapping of reagent in the sample, degradation/poisoning of the medium, and eventually, failure of a separation, catalytic process, or sensor device. Since single molecule tracking depicts the local behavior of molecules, and allows for spatial variations in the sample to be directly observed, it provides a path to investigating local diffusion rates in/on heterogeneous materials.

Diffusion coefficients for single molecules can be directly determined from the trajectories obtained from wide field imaging videos. Several different methods of determining diffusion coefficients from single molecule trajectory data have been reported, and are outlined below. McCain and Harris have reviewed some of these in earlier work. [63,64]

Scatter plots

One method suggested by McCain and Harris[63,64] is to use scatter plots showing the molecular step size and direction. In this method the individual trajectories are separated into single steps. A scatter plot is then drawn based on step size and direction, where the step size is the distance the molecule has traveled relative to its initial location. The distance of the spot from center represents the step size and the angle shows the direction of motion. The scatter plot is meaningful for directional bias checking but not very practical for quantitatively determining

diffusion coefficients. Determination of diffusion coefficients from such scatter plots requires either very long trajectories or averaging over a large number of trajectories to minimize the uncertainty.

Cumulative square displacement from the initial location versus time

Another method to determine diffusion coefficients from single molecule tracking data is to plot the time dependence of the cumulative square displacement from the initial location.[58] According to the Einstein equation for diffusion in two dimensions, $r^2=4Dt$, where D is the diffusion coefficient representing the rate of diffusion, t is the time and r is the radius. For ideal free diffusion, such a plot should provide the diffusion coefficient from the fitting line slope. But the fitting line may have a large uncertainty, which is due to shortcomings in the method itself. Because the molecule has a large probability of randomly walking back towards its initial location, the molecule can move closer to its initial location, resulting in a smaller cumulative square displacement, which leads to plots that have a significant deviation from linearity.

Mean square displacement of single trajectory versus time

The scatter plots and cumulative square displacement methods clearly have significant limitations in determining diffusion coefficient D. Therefore, researchers have instead started using single step (or multistep) mean square displacements to improve the precision of the measured D values. In this method, the individual steps are considered as independent diffusion events, starting at the previous location of the molecule. Thus, it does not matter if the molecule moves back to its initial location, it is only relevant how far it moves for the defined time step. Implementation for single frame time steps involves simply calculating the average squared displacement of the molecule between pairs of video frames.

For a molecule random walk, the MSD versus time plot should be linear with slope proportional to the diffusion coefficient. Figure 1-4 shows the experimental MSD versus time plot of three individual molecules in/on a silica dip-coating gradient film, diffusion coefficient was determined by the slope, $D=0.03\ \mu m^2/s$. Note that the molecule may exhibit directed motion or may move into a domain of greater mobility at long times, as is shown in the Figure 1-4, the data $D>0.03\ \mu m^2/s$. Here $D>0.03\ \mu m^2/s$ means that the molecule movers faster in time. Such behavior could be caused by molecules moving from a more viscous domain to a less viscous

domain, or by moving from a stronger bonding region to a less bonding environment, it can also by cased by external chemical/physical driving force.

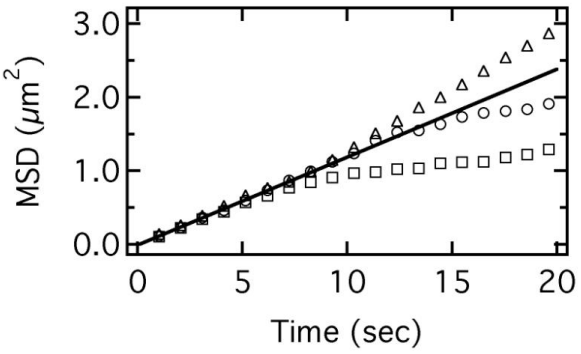

Figure 1-4. A MSD versus time plot of three individual molecules in/on a dip-coating silica thin film gradient.

Average mean square displacement of many single trajectories versus time

Because of the uncertainties in assigning single trajectory data to confined or super-diffusion, at present, the actual nature of diffusion can only be assessed on an ensemble basis, for trajectories of finite length. This can be accomplished by calcualting the average MSD from hundreds of trajectories. Figure 1-5 shows the MSD over hundruds trajectories vs time plot of a TMOS-MTMOS gradient sample. Different symbols represent different positions (2mm apart) on the film.

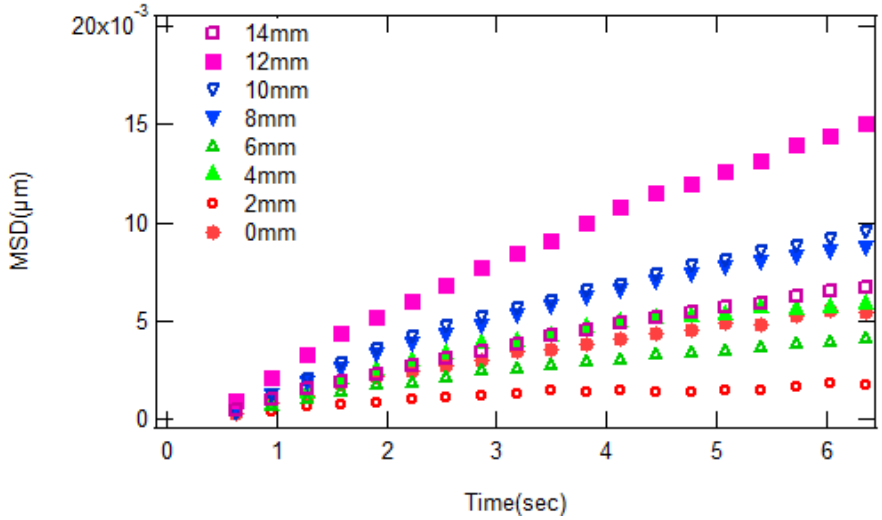

Figure 1-5. A MSD over hundruds trajectories vs time plot of a TMOS-MTMOS gradient sample.

The linearity of all the average MSD vs time slopes provides important evidence of dye molecule free diffusion within the sample. This method will be further discussed in Chapter 3 below.

Diffusion coefficient histogram

While the MSD versus time graph can be used to measure the diffusion coefficient directly from the slope, fitting the histogram of MSD or D to the expected distribution can also give a measurement of D, namely, the mean D value for an entire population of molecules. More importantly, the diffusion coefficient histogram reveals the distribution of diffusion coefficients. For example, Figure 1-6 shows the MSD histogram of one position on a TMOS-MTMOS gradient film. The MSD histogram depicts the presence of two population groups. The MSD histogram clearly shows one group of molecules is relatively fixed and the other group of molecules is mobile. The information shown on the MSD histogram was averaged out in the above MSD versus time method. The full histogram data is important in that it depicts the heterogeneity of the film.

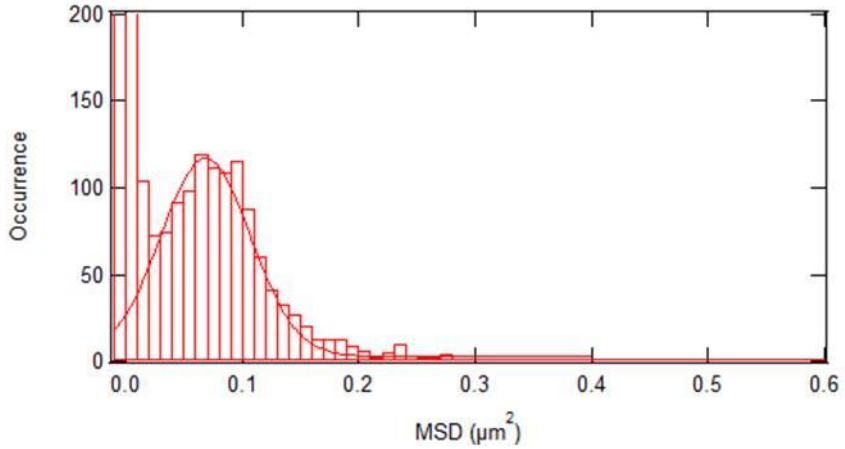

Figure 1-6. A MSD histogram of one position on a TMOS-MTMOS gradient film.

1.4 Conclusion

Silica materials have potential applications as stationary phases for chemical separations, as materials for combinatorial catalysis, and as absorbent/adsorbent layers for use in chemical or biological sensors. Related surface gradients have been used to investigate the preparation of silica materials. Information on film structure, film heterogeneity, and molecule mobility is important for a variety of applications. Single molecule tracking by wide-field microscopy

provides a way of tracking and studying molecular movements in thin film materials and understanding their nanoscale properties.

Chapter 2 - Experiment Section

2.1 Sample preparation

2.1.1 Preparation of silica thin films

2.1.1.1 Coverslip and silicon wafer sublayer

Glass coverslips (Fisher Premium) and silicon wafers (Silicon Inc.) were both employed as substrates. Prior to use, all substrates were cleaned in fresh Piranha solution (Caution, Piranha solutions are extremely dangerous and react violently with organic materials); they were subsequently cleaned a second time in an air plasma. This two-step process ensured rigorous removal of all organic contaminants, which, if present, led to poor adhesion of silica materials to the substrate surface.

2.1.1.2 TMOS-coated sublayer

Gradient films were found to be most uniform and adhered best to the substrate when deposited on a precast silica sublayer. Tetramethoxysilane (99%, TMOS, Aldrich) sols were employed for production of these sublayers. Briefly, TMOS, deionized water (HPLC grade, Acros), ethanol (200 proof, HPLC grade, Sigma-Aldrich) and HCl (ACS grade, Fisher) were mixed in a certain mole ratio in a clean glass vial. The sol was then aged at room temperature in a dessicator for 24 hours prior to use.

The sublayer sol (described above) was then spin coated onto the substrate. The sublayers were allowed to dry in a dessicator for 1 day prior to further use. Sublayer films created by this procedure were uniform and had thicknesses of 130~200 nm, as determined by both profilometry and spectroscopic ellipsometry.

2.1.1.3 Dip-cast and spin-cast non-gradient films on TMOS-coated sublayer

To verify the interpretations of data obtained from gradient films, silica films having uniform composition and derived from two different sols were also prepared. The first sol was a TMOS sol prepared in a 1:80:5.3:0.095 (TMOS: Ethanol: H_2O: NH_4OH) mole ratio and subsequently aged for 6 h. The second sol was any of several different sols prepared using

methyltrimethoxysilane (97%, MTMOS, Fisher). Typically, sols were prepared using different volumes of ethanol and constant water concentration. These sols were prepared in 1:10:4:0.072, 1:20:8:0.072, and 1:40: 13:0.072 (MTMOS:Ethanol:H_2O:NH_4OH(1 M)) mole ratios and were aged for 6 h.

The sol aging time was selected after experimentation with sols aged for both shorter and longer times. Shorter aging times yielded thinner films, whereas longer times yielded films of increased thickness and roughness. It was concluded that 6 h aging yielded the most acceptable films (i.e., of reasonable thickness and relatively small roughness).

Sols containing different molar fractions of TMOS and MTMOS were then obtained by mixing appropriate amounts of each of the above sols. Mixed sols containing 0%, 20%, 40%, 60%, 80% and 100% MTMOS (relative to total silica content) were prepared and vigorously mixed for 20 min. These sol mixtures were then dip cast and spin cast in separate film preparations onto both clean and sublayer-coated substrates.

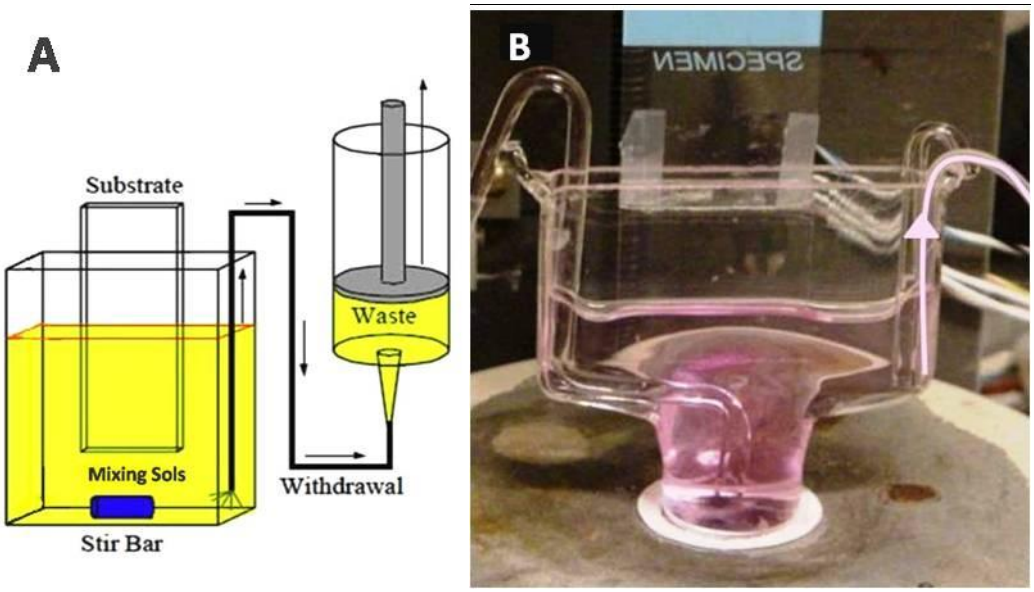

Figure 2-1. A) A diagram of non-gradient dip-coating apparatus and B) a photograph of the reservoir used for dip-coating.

Dip-cast non-gradient films were deposited on the TMOS sublayer-coated substrates in a custom built glass reservoir designed to simultaneously minimize sol volume, decrease sol evaporation and allow for stirring of the sol mixture. A diagram of the apparatus and a photograph of the reservoir are shown in Figure 2-1. The glass reservoir includes a rectangular upper region having dimensions of 3.5cm ×0.5cm ×3.0cm (L ×W ×H) that was designed to

admit one inch wide substrates. The lower portion of the reservoir was comprised of a small cylindrical vial (D=1cm, H=1cm). Small glass tubes were installed at fixed locations inside the reservoir for withdrawal of the sols.

Figure 2-2. New Era Pump Systems syringe pump.

A syringe pump was used to withdraw the sol from the deposition reservoir during dip coating (rather than withdrawing the substrate from the reservoir). For this purpose, a syringe was attached to the reservoir via flexible plastic tubing, which was mounted in the syringe pump (NE-1000, New Era Pump Systems, Inc.) shown as Figure 2-2. Dip cast non-gradient deposition proceeded by slowly withdrawing the stirred sol from the reservoir into the syringe. The withdraw pump rate was set to 10.0 mL/h, so a 16 mm non-gradient film was deposited on TMOS-coated substrate in ~45 min. After deposition, residual sol clinging to the bottom of the substrate was gently removed using a Kimwipe. All depositions were performed with the reservoir mounted atop a pneumatic vibration isolation table, and with the reservoir housed in a closed Plexiglas box maintained at ~50% relative humidity and ~20 ℃.

Spin-cast non-gradient films were made by spin casting mixed sols onto TMOS sublayer-coated substrates at a spin rate of 5000 rpm. All dip-cast and spin-cast films were dried in a vacuum dessicator at room temperature for 1~ 2 days prior to use.

2.1.2 Preparation of silica thin film gradient

Gradient films were obtained by methods similar to the preparation of non-gradient films. Briefly, silica gradients were created by first preparing separate TMOS and MTMOS sols. Either a one step base or two-step acid-base hydrolysis and condensation procedure was used in preparation of each sol. The sols employed were initially hydrolyzed and condensed in separate

vessels. As shown by both our group [65-67] and others[68], the mixing and subsequent deposition of such separately-hydrolyzed sols can produce heterogeneous films comprised of "phase separated" domains of the individual silica components.

2.1.2.1 One-step base hydrolysis and condensation procedure

One step base hydrolysis and condensation was employed for preparation of films in the early phases of work performed for this thesis. Typically, in the one step base hydrolysis and condensation procedure, TMOS sols were made in a 1:80:5.3:0.095 (TMOS: Ethanol: H_2O: NH_4OH) mole ratio and subsequently aged for 6 h, and MTMOS sols were made in a 1: 40: 13: 0.072 (MTMOS: Ethanol: H_2O: NH_4OH) mole ratios and aged for 6 h. The appropriate aging time was selected as described above.

Deposition of silica film polarity gradients was accomplished as follows. A sublayer-coated substrate was first suspended in the middle of the reservoir. The initial TMOS sol was then transferred into the reservoir, submersing all but the top 1-2 mm of the substrate. The MTMOS sol selected for a given deposition was then loaded into a syringe and mounted in a syringe pump (Figure 2-2). The syringe was attached to the reservoir via flexible plastic tubing. Gradient deposition proceeded by slowly infusing the MTMOS sol into the reservoir. The mixed sol contained in the reservoir was simultaneously withdrawn using a second, synchronized syringe pump also attached to the reservoir through flexible plastic tubing. The infusion pump was set to deliver MTMOS sol at a rate of 10.0 mL/h, while the other was set to withdraw 14.2 mL/h of mixed sol. The sol within the reservoir was carefully stirred at a constant rate, using a magnetic stir bar throughout this process, as shown in Figure 2-3. Prior to the start of deposition, it was verified that sol stirring produced no detectable movement of the sol surface. The difference in infusion and withdrawal rates led to a steady decrease in the height (~ 0.3 mm/min) of the sol in the reservoir. The entire "infusion-withdrawal dip-coating" process lasted for ~ 1 h, producing an overall change of ~ 1.8 cm in sol height. After deposition, residual sol clinging to the bottom of the substrate was gently removed using a Kimwipe. The final gradient films were dried in a dessicator for 1~ 2 days. In some cases, gradients were simultaneously prepared on two coverslips, using the same sol mixture. In this case, the two substrates were assembled back-to-back with a thin film of glycerin between them. The thin layer of glycerin prevented silica deposition on the backside of the substrates.

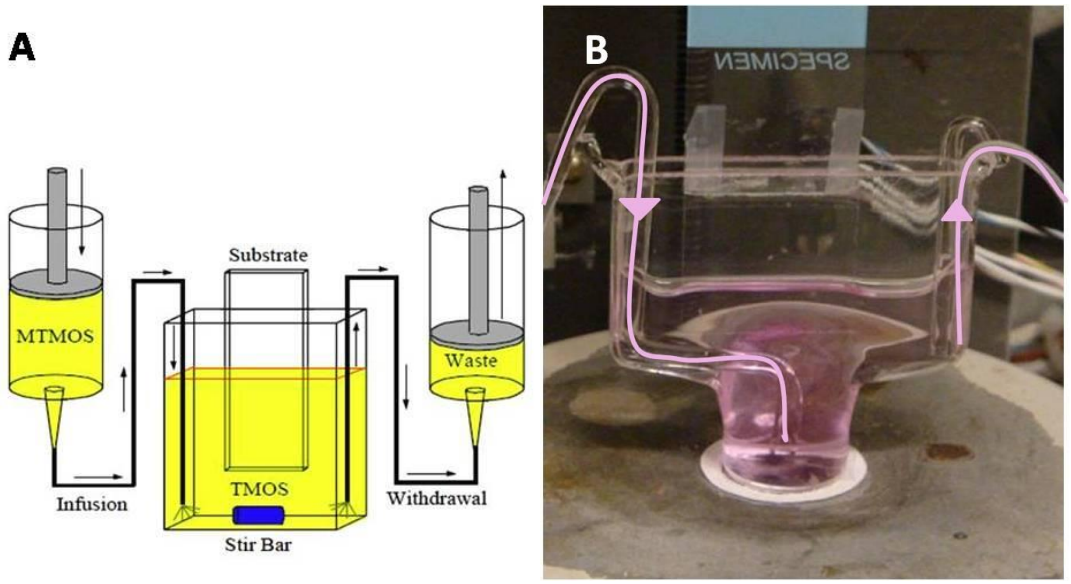

Figure 2-3. A) A diagram and B) photograph of "Infusion withdraw dip-coating" apparatus.

2.1.2.2 Two-step acid-base hydrolysis and condensation procedure

A two-step acid-base hydrolysis and condensation procedure was implemented in later gradient preparation because this method produced better uniform film with more methyl content in gradient. Thus, the gradient was thin enough for single molecule study, and still with gradually increasing methyl content in it. In the two-step acid base hydrolysis and condensation procedure, gradients were obtained by methods similar to those described above. Briefly, silica gradients were created by first preparing separate TMOS and MTMOS sols. A two-step acid-base hydrolysis and condensation procedure was then used in both cases. TMOS sols were made in a 1.00:138.94:9.37:0.01:0.08(TMOS: Ethanol: H_2O: HCl: NH_4OH) mole ratio while MTMOS sols were made in a 1.00:134.36:9.06:0.01:0.08 (MTMOS: Ethanol: H_2O: HCl: NH_4OH) mole ratio. In the two-step acid-base process, the silane, ethanol and HCl were first mixed together by stirring for 5 min (TMOS) or 10 min (MTMOS). The NH_4OH was added into the mixture at this point, as was Nile Red, for preparation of dye-doped sols (see Section 2.1.2.3). Stirring was then continued for an additional 30 min. The sols were then allowed to age in a dessicator for an additional 80 min, yielding a total stirring/curing time of 2 hrs.

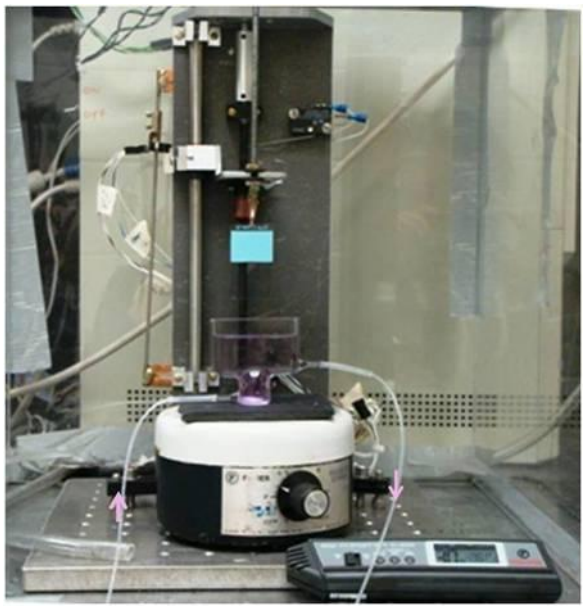

Figure 2-4. A photograph of two-step acid base dip-coating gradient apparatus.

During gradient deposition, the sublayer-coated substrates were suspended in the deposition reservoir,[1] which was subsequently filled with the TMOS sol. The reservoir inlet tube was connected to a syringe pump and the syringe was filled with the MTMOS sol. The reservoir outlet was connected to a second syringe pump holding an empty syringe. A small magnetic stir bar positioned at the bottom of the reservoir, near the inlet, was used to stir the sol throughout the dip-coating process. The entire apparatus was housed in a humidity control chamber, which was used to maintain ~ 50% relative humidity (RH) during film deposition (Figure 2-4). Infusion of the MTMOS sol and withdrawal of the mixed sol were initiated as soon as the atmosphere in the humidity chamber had stabilized. Withdrawal of the substrate from the deposition reservoir, using a computer controlled stepper motor, was also initiated at this same time. Sol infusion and withdrawal were set at identical rates and were maintained at these rates throughout gradient deposition. Note that this dip coating procedure differs somewhat from the procedure described for the one step base process. Although implementation of a stepper motor was required for substrate withdrawal, the change in procedure allowed for more reproducible deposition of gradients having well controlled lengths. The full deposition procedure (from initiation of infusion and withdrawal until the substrate had been fully extracted from the reservoir) took 45 min. Gradients ~14 mm in length were prepared. All samples were dried in an opaque vacuum dessicator for at least 24 h before further use. Films employed in single molecule studies were

dried for 1, 3 and 5 d so that the impacts of film aging on the film properties could be investigated.

2.1.2.3 Preparation of dye-doped silica gradients

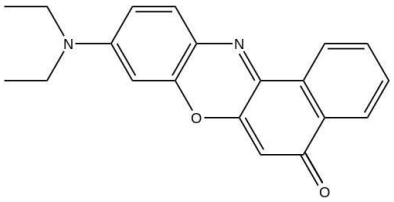

Figure 2-5. Nile Red chemical structure.

Preparation of dye-doped silica gradients was performed only on glass coverslips and preceded exactly as described above. The dye used in the experiments was Nile Red, which is a strongly polarity sensitive fluorescent probe. Its chemical formula is shown as Figure 2-5. Gradients were doped into the sols at concentrations of 1μM for bulk studies of silica film gradients and at concentrations of 0.1nM for single molecule studies.

2.2 Instrumentation

2.2.1 Bulk fluorescence spectroscopy

Fluorescence spectra were obtained from Nile Red-doped gradients and spin-coated films using a home-built fluorescence microscope (Figure 2-6). Light (~1 μW) from a green HeNe laser (543.5 nm) was used to excite fluorescence in the samples. This light was focused into the back aperture of a 40X dry objective, producing a 20 μm diameter spot in the sample. The same objective was used to collect the sample fluorescence and direct it through a 543 nm holographic notch filter (Kaiser Optical) and into a 0.15 m spectrograph (Acton Research). A liquid-N2-cooled CCD (Princeton Instruments) was used to record the spectra. Spectra were acquired every 1(±0.2) mm along the gradient, using a 30 s integration time.

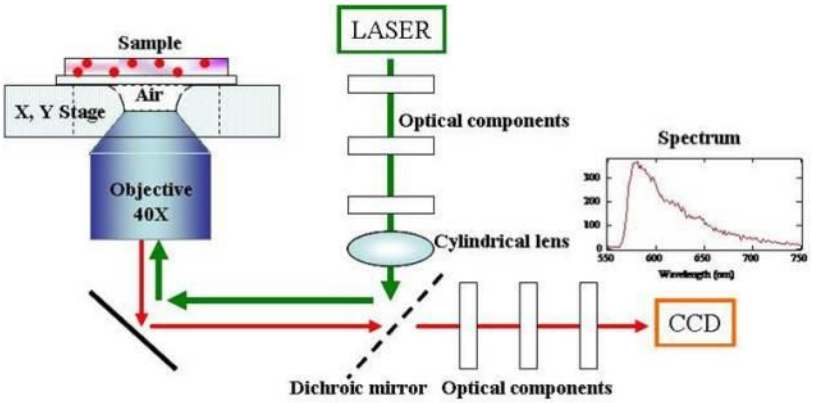

Figure 2-6. A diagram of fluorescence microscopy.

2.2.2 Wide-field microscopy

Fluorescence images of gradient films doped with Nile Red at 0.1nM concentrations were acquired on a wide-field fluorescence microscope. This system was built upon an inverted epi-illumination microscope as depicted in Figure 2-7.

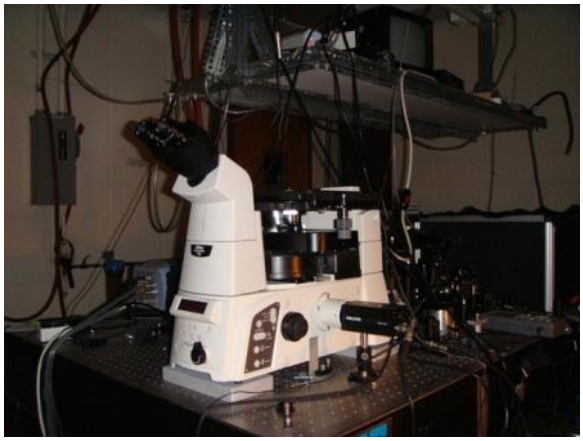

Figure 2-7. Nikon Eclipse Ti microscope.

The diagram of wide field microscopy setup is shown in Figure 2-8. Light from a Nd:YVO_4 laser (532nm) was used to excite Nile Red fluorescence in the sample. It was delivered to the microscope via an optical fiber and was subsequently passed through an electronic shutter and additional optics for regulating the power incident on the sample. The light was then focused into a spinning optical diffuser and was subsequently collected and passed through a polarization scrambler and into the epi-illumination port of the microscope. Inside the microscope, the light was reflected from a dichroic beamsplitter (Chroma Q555LP) and was focused into the back aperture of an oil immersion objective (Nikon Apo TIRF 100x, 1.49

numerical aperture/N.A.). The incident laser power was commonly maintained at ~1.0 mW (estimated from measurements made just prior to the dichroic beamsplitter). Samples used in all single molecule experiments were supported on glass coverslips. Fluorescence from the sample films was collected in reflection and was separated from the excitation light by passage back through the dichroic beamsplitter and through a bandpass filter (Chroma HQ610/75m). A back-illuminated electron multiplying charge-coupled device (EM-CCD) camera (Andor iXon DU-897) was used as the detector.

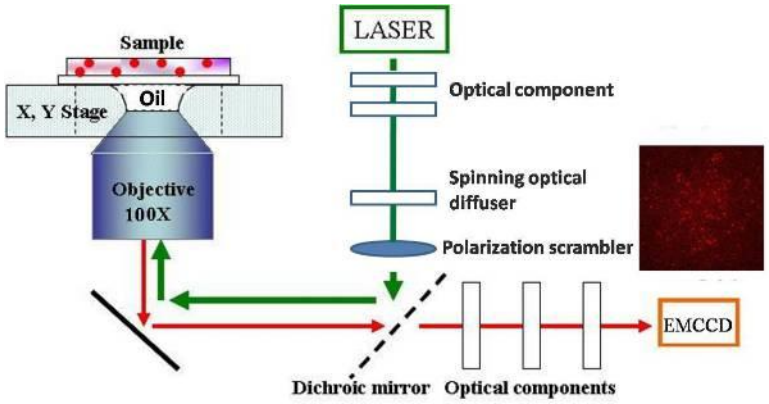

Figure 2-8. A diagram of wide-field microscopey.

Wide-field movies were commonly recorded as 500 frame videos with 1.03 s frame times. The image area was comprised of 256 pixels x 256 pixels, corresponding to a 44 μm x 44 μm (1 pixel = 0.17 μm) region in the sample. Calibration of the size of the region imaged was accomplished by comparing the size of 1 μm diameter sphere with the pixel size in the wide-field image. All videos were acquired under a N_2 atmosphere, at a relative humidity (RH) of ~30%; the same RH atmosphere was maintained for the duration of all experiments. Videos were acquired at 2 (±0.2) mm intervals along each gradient. Three separate videos were acquired from parallel positions at each point.

2.2.3 Static sessile-drop water contact angle measurements

Static sessile-drop water contact angle measurements were performed on a home-built apparatus (Law labs, KSU Physics) run by software written in-house, as shown Figure 2-9. A Navitar camera was used to record droplet images. In these experiments, 2.5 μL drops of deionized water were deposited at regular intervals on the samples. Images were acquired 3 s after addition of each drop to the sample surface, allowing for stabilization of the contact angle.

Automated routines incorporated into the instrument software were used to determine contact angles.

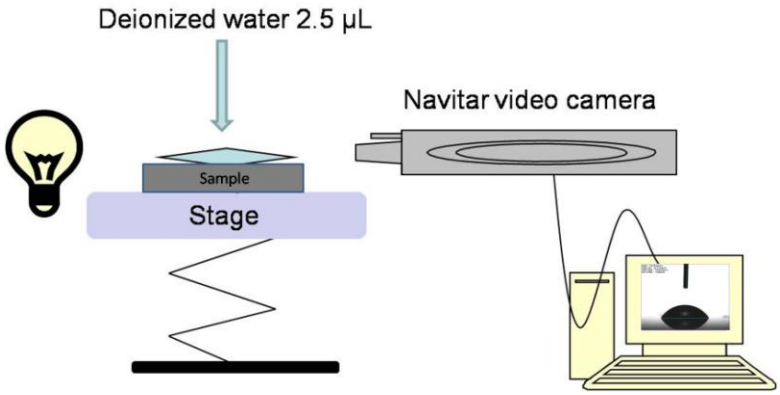

Figure 2-9. A diagram of the water contact angle setup.

2.2.4 Spectroscopic ellipsometry and profilometry

Film thicknesses for the sublayers and gradients were determined by spectroscopic ellipsometry (α-SE, J. A. Woollam, Ito labs, KSU Chemistry) and by surface profilometry (XP-2, Ambios Technology, Culbertson labs, KSU Chemistry). All measurements were performed on silicon-supported films.

Spectroscopic ellipsometry has been employed previously for characterization of film thickness and optical constants in multilayer[69] and nonuniform gradient[70] films. To determine film thickness as a function of position, ellipsometric data were acquired at 1(0.2 mm intervals along the films. Three measurements were taken every 1(±0.2) mm. Data were acquired from approximately the same locations (i.e., within (0.2 mm) both before (TMOS sublayer alone) and after gradient deposition. The films were modeled as transparent layers on silicon, with dispersion in the films described by the Cauchy relationship.[69] Data obtained from TMOS sublayers alone could all be modeled with similar parameters (e.g., Cauchy A parameter =1.426, B = 0.00698, and C = -0.00049). The gradient overlayers were modeled as a second layer atop the TMOS sublayer (Cauchy A parameter =1.25, with B, C, with the gradient thickness adjusted to fit the data). In all cases, the film thickness values determined by ellipsometry were consistent with those obtained from profilometry measurements.

Profilometry measurements of gradient surface roughness and film thickness were accomplished by either scanning along gradient or making a deep but narrow (~50 µm) scratch

in the gradient film on TMOS coated Si substrate, then scanning across the scratch to measure the depth of scratch from the scanning profile.

2.2.5 Transmission-mode FTIR microscopy

Transmission-mode FTIR microscopy was performed on a Thermoelectron FTIR Continuum Microscope coupled to a Nexus 670 spectrometer (Collinson labs, Chemistry, Virginia Commonwealth University). Films characterized by FTIR microscopy were also prepared on silicon substrates. Spectroscopic imaging was accomplished by averaging 1000 interferometer scans at each position along the gradient, using a 150 x 150 μm^2 imaging aperture. All spectra were baseline corrected. A TMOS-sublayer-coated silicon slide was used for the background.

All FTIR microscopy measurements were made by Balamurali Kannan at Virginia Commonwealth University.

Chapter 3 - Results and Discussion

Two journal articles have been published based on the work described in this chapter. The work is reprinted with permission from the American Chemical Society.

1) Chenchen Cui, Alec Kirkeminde, Balamurali Kannan, Maryanne M. Collinson and Daniel A. Higgins. "Spatiotemporal Evolution of Fixed and Mobile Dopant Population in Silica Thin-Film Gradients as Revealed by Single Molecule Tracking." *J. Phys. Chem. C* **2011**, *115* 728-735. Copyright 2011, American Chemical Society.
2) Fangmao Ye, Chenchen Cui, Alec Kirkeminde, Dong Dong, Maryanne M. Collinson and Daniel A. Higgins. "Fluorescence Spectroscopy Studies of Silica Film Polarity Gradients Prepared by Infusion-Withdrawal Dip-Coating." *Chem. Mater.* **2010**, *22*, 2970-2977. Copyright 2010, American Chemical Society.

3.1 Bulk studies of polarity gradients in silica thin films

Silica films prepared from mixtures of inorganic (TMOS) and organically modified (MTMOS) silica precursors represent a valuable route to materials of controlled polarity properties. Such materials may have applications as membranes for chemical separations by partitioning or for optimization of energy transfer in materials for solar energy conversion. Preparation of continuous polarity gradient films by infusion withdrawal dip coating represents an efficient means for preparing and characterizing materials with a wide range of polarity properties. In these experiments, the polarity properties of the gradients were probed primarily by bulk fluorescence spectroscopy, using a strongly polarity sensitive fluorescent probe, Nile Red.

3.1.1 Preparation of silica film gradients

The "infusion-withdrawal dip-coating" process is employed for the preparation silica thin film gradients. Briefly, glass and silicon substrates were coated with sols of time-varying composition produced by slowly mixing TMOS- and MTMOS-based sols together. The time-varying sol composition led to a steady increase in methyl content along the substrate surface. A more detailed discussion of the preparation of these films is given in Chapter 2 of this thesis.

3.1.2 Optical inspection of films

Optical inspection was employed to judge the overall quality of the gradient films obtained. Figure 3-1A shows a representative photograph of a gradient on a sublayer-coated silicon substrate. This particular film was derived from a MTMOS to ethanol mole ratios 1:40 MTMOS sol. It is 1.3 cm wide and the gradient is 1.6 cm in length. It is most noteworthy that a general trend from dark to light is observed from top to bottom along the gradient film. Unfortunately, colorful interference lines are also observed. These run across the film (i.e. perpendicular to the gradient dimension) and appear at "random" locations along the gradient. These lines have been shown previously to arise by a "stick-slip" process at the sol-substrate contact line during film deposition.[1]

3.1.3 Thickness and surface roughness

The thicknesses of the TMOS sublayers and gradient films cast on silicon substrates were determined using spectroscopic ellipsometry. Film thickness was measured at 1 mm intervals both before and after gradient deposition in approximately the same locations (i.e., within (0.2 mm) in each case. Figure 3-1B shows representative position-dependent thickness data acquired from a gradient prepared by MTMOS to ethanol mole ratio 1:40 MTMOS sol. Shown are thickness values for the overall film, the TMOS sublayer, and the gradient itself. Surface profilometry measurements performed on similarly prepared films yielded thickness values consistent with all ellipsometry data. These data show that the TMOS sublayer is relatively uniform across the substrate and 180 nm thick. The gradient film, however, shows a clear decrease in average thickness along the gradient dimension. In this sample, the gradient film thickness is greatest at the top, yielding a value of 140 nm, and gradually decreases to ~40 nm thick at the bottom.

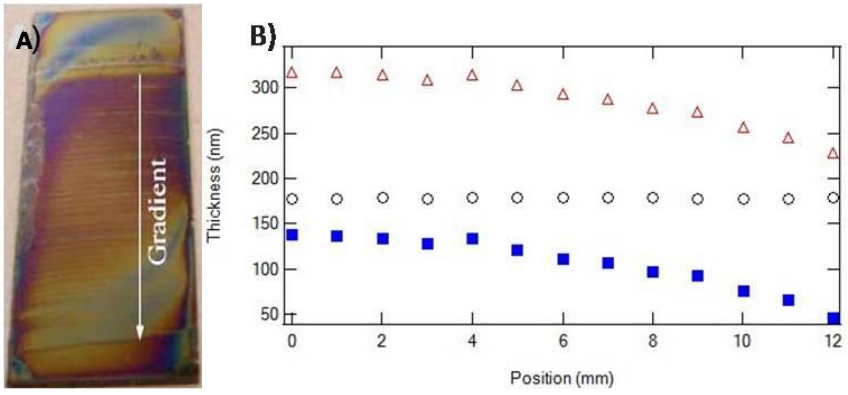

Figure 3-1. A) A photograph of a gradient on a sublayer-coated silicon substrate B) Position-dependent thickness determined by ellipsometry for a gradient prepared by "infusion-withdrawal dip-coating" using a MTMOS to ethanol mole ratio 1:40 MTMOS sol, overall film thickness (open triangles), thickness of TMOS-coated substrate (open circles), and gradient thickness (solid squares) are shown.

Film thinning is partly a result of variations in the influence of stirring (as the deposition region gradually approaches the stir bar) but could also include contributions from differences in the wetting of the sublayer by the time varying mixed sol, differences in the degrees of hydrolysis and condensation of TMOS and MTMOS, differences in the rates at which these two precursors attach to the sublayer, or differences in the sol viscosities.[71,72]

3.1.4 Water contact angle

Strong evidence for the formation of methyl-modified silica film gradients was obtained from sessile-drop water contact angle measurements.[73-76] The incorporation of methyl groups in sol-gel materials derived from MTMOS makes them more hydrophobic than those prepared from TMOS alone, leading to an expected increase in contact angle running down the gradient.

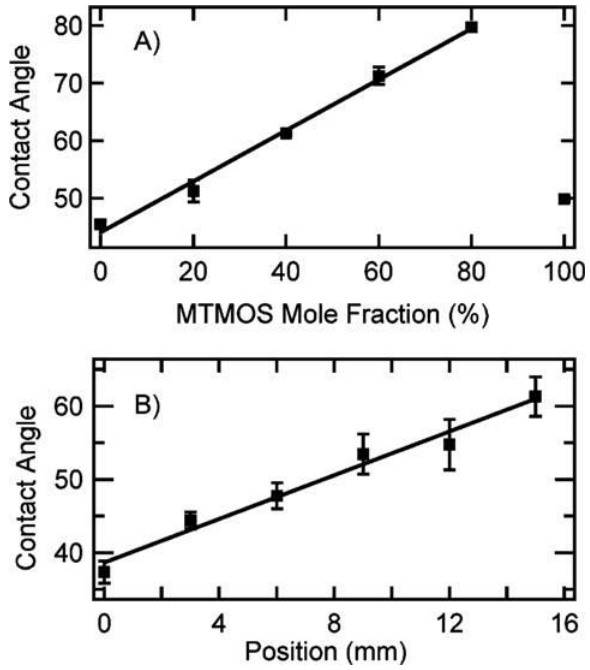

Figure 3-2. Contact angle in degrees for A) one- and two-component non-gradient (dip-coated) films and B) a gradient prepared by MTMOS to ethanol mole ratio 1:40 MTMOS sol, both on TMOS sublayer-coated substrates. The solid lines have been added to better

depict trends in the data. The error bars show the standard deviations obtained from multiple measurements performed on each sample.

Variations in the contact angle attributable to methyl modification were initially explored for one- and two- component non-gradient films (dip-coated and spin-coated on TMOS-sublayer-coated substrates) prepared from sols of differing MTMOS and TMOS mole fractions. The results for dip-coated films are plotted in Figure 3-2A. A monotonic increase in water contact angle was observed for films derived from 0% to 80% MTMOS sols. For pure TMOS, the water contact angle was 45^{o}, whereas for 80% MTMOS, it was 80^{o}. A similar trend was observed for spin-coated non-gradient films. These contact angle values are consistent with those reported previously for related "nonporous" sol-gel derived silica films,[77-79] but are significantly smaller than those of porous MTMOS-derived superhydrophobic aerogels.[80,81] Deviation from the observed trend at 100% MTMOS is attributed to the formation of nonuniform/discontinuous films in this case. Film nonuniformity is evidenced by increased film roughness that is observable by eye.

Water contact angles were also measured as a function of position along each of the silica film gradients. Figure 3-2B plots representative contact angle results for a gradient prepared by MTMOS to ethanol mole ratio 1:40 MTMOS sol. The gradient film shows a monotonic trend similar to that obtained from the non-gradient films, exhibiting contact angles of 37^{o} at the top of the gradient, and 61^{o} at the bottom. These data are consistent with the presence of a methyl-modified silica gradient running from top to bottom. The differences in contact angles obtained from gradient and non-gradient films are attributed to differences in the preparation methods (i.e., time-varying sol mixtures in the former, homogeneous mixtures in the latter) and differences in surface roughness. It is well known that variations in surface roughness can cause variations in the contact angle,[82,83] making quantitative comparisons between data sets difficult. Surface roughness specifically leads to observed contact angles that are smaller and larger, respectively, than expected on hydrophilic and hydrophobic surfaces.[82,83] Profilometry data shows the roughness is ~50% greater at the top of the gradient than at the bottom, suggesting the contact angles at the top of the gradient may be depressed due to increased roughness. It is concluded that although roughness variations may enhance the trend in contact angle along the gradients, these data remain consistent with the presence of a polarity gradient.

3.1.5 Fluorescence measurements of film polarity

The primary objective of the present work is to produce silica films incorporating polarity gradients. Polarity along the gradient direction in films prepared as described above was probed by entrapping the solvent-sensitive dye Nile Red in the film. Nile Red has been used in the past to probe the polarity properties of a wide range of liquid and solid environments.[35,48,84-86] It is one of the most solvent sensitive fluorescent probes, exhibiting a dramatic bathochromic shift (of ~100 nm) in its emission spectrum between nonpolar (i.e., hexane) and polar (i.e., water) solvents.[84] In the present experiments, Nile Red was doped into both gradient and non-gradient silica films at ~1 μM concentrations.

3.1.5.1 Nile Red emission from non-gradient films

Nile Red emission spectra were initially recorded for a series of non-gradient TMOS and MTMOS films. These experiments provided valuable information on its emission characteristics for films of different polarities. Emission spectra were first acquired from single-component, non-gradient films that had been prepared on TMOS sublayer-coated coverslips using dip-coating methods similar to those used in gradient preparation (see Chapter 2). The fluorescence emission maxima for TMOS and MTMOS derived films appeared at ~640 and ~618 nm, respectively, reflecting the significant polarity differences of these films. These emission maxima were found to be similar to those obtained from spin-coated TMOS and MTMOS films prepared both without and with TMOS sublayers (~ 650 and ~605 nm, and ~643 and ~615 nm, respectively). The shift in Nile Red emission between spincoated MTMOS films prepared without sublayers and those obtained by dip-coating on TMOS sublayers show that penetration of Nile Red into the sublayer has only a modest effect on the results.

A series of one- and two-component, non-gradient silica films derived from 0, 20, 40, 60, 80, and 100% MTMOS sols (relative to total silane) were also investigated. Emission spectra obtained as a function of MTMOS mole fraction in the non-gradient films provide a clear view of the hypsochromic shift exhibited by Nile Red upon a change from TMOS-derived films to MTMOS-derived films. In order to more quantitatively assess the polarity characteristics observed for films prepared using different TMOS and MTMOS mole fractions, a "polarity fraction" (PF) was defined. The PF was calculated directly from the Nile Red emission spectra by measuring the average Nile Red fluorescence in 10 nm wide bands centered at 605 nm

(reflecting nonpolar environments) and 650 nm (polar environments) and determining the fraction of the total emission that occurred in the 605 nm band, as given in Eqn. 3.1.

$$R_{MTMOS(t)} = \frac{C_{MTOMS(t)}}{C_{MTOMS(t)} + C_{TMOS(t)}} \tag{3.1}$$

The PF is expected to increase with increasing methyl content of the films. PF values of 0.25 and 0.60 were obtained for non-gradient spin-coated TMOS and MTMOS films (without sublayers), respectively.

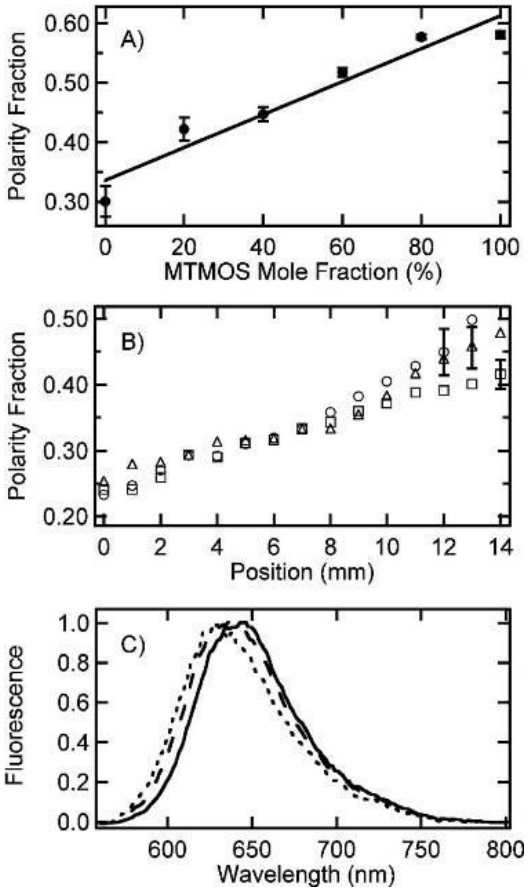

Figure 3-3. A) Polarity fraction (PF) as a function of MTMOS mole fraction for one- and two-component non-gradient (dip-coated) films. The solid line has been appended to better depict the trend in the data. B) Polarity fraction as a function of position for gradient samples. The top of the gradient corresponds to 0 mm. Shown are data from gradients prepared by MTMOS to ethanol mole ratio 1:10 (open squares), 1:20 (open triangles) and (open circles) MTMOS sol. The error bars represent the average standard deviation obtained from measurements on at least three different samples in each case. C)

Representative Nile Red fluorescence spectra (normalized) for a gradient prepared by MTMOS to ethanol 1:10 MTMOS sol taken from the top (solid line), middle (dashed line), and bottom (dotted line) of the gradient.

Figure 3-3A plots the PF values obtained as a function of MTMOS mole fraction in non-gradient films dip-coated onto TMOS-sublayer-coated substrates. A monotonic and nominally linear increase from 0.30 to 0.58 is observed in the PF value as the mole fraction of MTMOS in the dipping sol increases from 0 to 80%. The similarities in the PF values obtained from spin-coated and dip-coated films in the absence and presence, respectively, of a TMOS sublayer provides supporting evidence that the polarity results are not dramatically altered by penetration of the dye into the TMOS sublayer.

3.1.5.2 Nile Red emission from gradient films

Nile Red spectra recorded from the gradient films clearly demonstrate the presence of a polarity gradient. The PF values obtained as a function of position along each of three different gradients are plotted in Figure 3-3B. Representative Nile Red fluorescence spectra are shown in Figure 3-3C. The PF data show a clear monotonic increase from the top (0 mm) of the film to the bottom. The PF values obtained from the gradients are somewhat smaller than those of the dip-coated non-gradient films. For example, the MTMOS to ethanol mole ratio 1:10 gradient exhibits an initial PF of 0.24, while a non-gradient 0% MTMOS (100% TMOS) film yields 0.30. At the other end of the same gradient, a PF of 0.42 is obtained, whereas a non-gradient 80% MTMOS film yields 0.58. These results suggest the gradient films are somewhat more polar than the non-gradient films. These polarity differences likely result from differences in the deposition process in each case. The non-gradient films are deposited from a static, homogeneous mixture of two sols, whereas the gradients are deposited from a time varying mixture, which never exactly duplicates the conditions under which the non-gradient films were deposited. Nevertheless, all three gradients (see Figure 3-3B) show PF values that are similar to those of the non-gradient films, suggesting similar variations in the methyl content of the gradients.

Interestingly, all three gradients show similar PF values (within experimental error) along their lengths, although the measured values become more variable toward the bottom of the gradients (see Figure 3-3B). The compositions of the sol mixtures from which the films were

grown are expected to be distinctly different, with higher MTMOS concentrations leading to greater methyl content at intermediate times. Such differences in the sol composition would be expected to appear in the final films as well, with greater methyl content observed in intermediate gradient regions, when relatively high concentration MTMOS sols are employed. The apparent insensitivity of the gradients to MTMOS concentration is again attributable to the details of silica deposition. Differences in the MTMOS sols arise primarily from dilution with ethanol. Because ethanol evaporation occurs efficiently from the top of the meniscus, [71] the concentration of silica precursor in the deposition region is likely more similar than otherwise expected from the composition of the original sol. As a result, little dependence of the final film properties (PF) on sol concentration is observed.

3.2 Single molecule study on silica thin film gradient

In the following study, single molecule methods were used to probe molecular mobility (i.e. Brownian motion) in and on silica polarity gradients that were virtually identical to those described in section 3.1.

3.2.1 Preparation of gradients

In this set of experiments, a two-step acid-base hydrolysis and condensation procedure was used in preparation of silica thin film gradients. A detailed discussion of gradient preparation by this method is given in Chapter 2. The two-step acid-base hydrolysis and condensation was employed here because it was shown to more efficiently deposit MTMOS content in TMOS-MTMOS gradients. It also led to more reproducible production of more uniform films. Gradients with measurable (by FTIR microscopy) MTMOS content could be made by this method. Films of reproducible ~ sub-100 nm thicknesses could also be prepared. Obtaining thinner films was crucial to performing single molecule studies. To successfully detect single molecules, the molecules must be spatially isolated from each other and must be present in higher concentration than any fluorescent impurities also present. The small detection volume makes it possible to detect the fluorescence from one molecule at a time[50], while limiting the probability that impurities appear in the detection volume and minimizing background due to scattering.

3.2.1 Film thickness

TMOS sublayer thicknesses were measured prior to deposition of the gradient overlayer. Film thickness was obtained by fitting the ellipsometry data to a "transparent film on silicon" model, with dispersion in the films described by the Cauchy relationship.[69] Full film thickness (sublayer plus overlayer) was obtained after gradient deposition, using the same model. The fits generated average Cauchy A parameters of 1.440(±0.003) and 1.436(±0.010) for the sublayer and full film, respectively. Note that the thinner gradient overlayer could be fit with similar A values as the sublayer in this case. However, these values suggest the presence of some residual water (~4-6% by volume) in the films.[71] The B (0.003 and 0.005) and C ($7x10^{-5}$ and $-4x10^{-5}$) values were relatively more variable (errors similar to average values), as required to properly fit the data. The gradient thickness was determined by subtracting the sublayer thickness from the full film thickness at each point. The region near the start of the gradient (i.e., within 1 mm) was often thick and rough, making it difficult to fit the ellipsometry data at this location. Excessive film thickness and roughness at the top of the gradient was attributed to the relatively long (~ 1 min) static exposure of this region to the sol, prior to the start of gradient deposition. The start of the gradient was defined as the first point below this region at which the ellipsometry data could be properly fit. Film thicknesses were confirmed by surface profilomery.

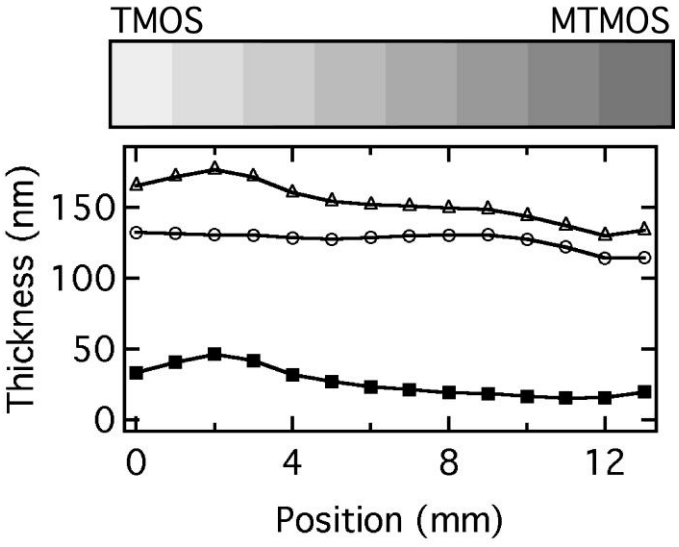

Figure 3-4. Top) Diagram of gradient film incorporating a gradual increase in methyl-modified silica content from top (0 mm) to bottom. Bottom) Film thicknesses determined by spectroscopic ellipsometry. Shown are data for the TMOS sublayer (open circles), sublayer-supported gradient (open triangles) and gradient film (filled squares).

Figure 3-4 depicts representative ellipsometric film thickness data obtained along one gradient. These data show the presence of a relatively uniform sublayer, having a thickness of ~ 130 nm. Deposition of the gradient overlayer yields a film in which the thickness decreases gradually from a maximum of ~ 175 nm near the start of the gradient to ~ 130 nm near its end. Control experiments in which the sublayer-coated substrate was dipped in the absence of precursor silanes demonstrate that the sublayer thickness did not change (e.g., the sublayer is neither dissolved nor swelled) during dip-coating. Subtraction of the sublayer thickness from that of the full film demonstrates the presence of a gradient overlayer that gradually thins from ~ 45 nm to ~ 15 nm. Fitting the data to a two-layer model, as was done previously (see Section 3.1), yielded uniformly larger gradient thicknesses (by ~ 5 nm), a difference well within the error of profilometry measurements used to verify film thickness. More significant film thinning was found previously, as discussed in Section 3.1.[87] Thinning likely arises from reduced reactivity of the MTMOS sol with the sublayer surface. In the present implementation, film uniformity was greatly improved (i.e., thinning was less severe) by use of the acid-base two-step hydrolysis and condensation process. Gradient overlayer thickness also varied on sub-millimeter length scales, as observed by surface profilometry for the same reasons described in Section 3.1.

3.2.2 FTIR microscopy

Evidence for the creation of a TMOS-MTMOS gradient exhibiting a gradual increase in film methyl content was obtained by FTIR microscopy. Gradients for IR microscopy were prepared from sols having twice the concentration of those used in ellipsometry and fluorescence experiments. The films obtained were approximately twice as thick as the others. Thicker films were required here because IR absorption in the relevant spectral regions was found to be too weak for the thinner films.

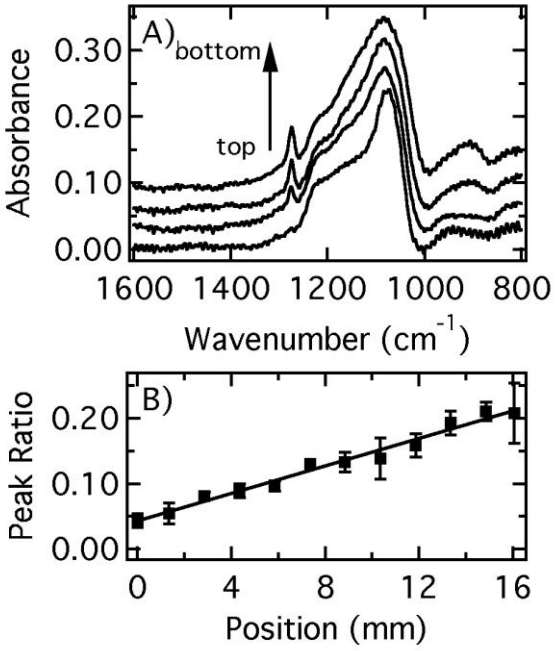

Figure 3-5. A) Representative FTIR spectra recorded along a silica film gradient supported on a TMOS-coated silicon substrate. The spectra have been baseline corrected, smoothed and offset vertically to more clearly depict peak height trends from the top (TMOS) to bottom (MTMOS) of the gradient. The peak at 1275 cm^{-1} ($Si-CH_3$) is diagnostic for methyl-modified silica. The peak at 1080 cm^{-1} (Si-O-Si) provides an approximate means to correct for film thickness variations. B) Average peak height ratio ($Si-CH_3$/Si-O-Si) as a function of position along the gradient (0 mm = top, TMOS). The concentrations of the sols used in preparation of this gradient were twice that of those used for single molecule studies. Each point depicts the average value (and standard deviation) obtained from three spectra obtained from neighboring positions. All FTIR microscopy data was acquired by Balamurali Kannan, Virginia Commonwealth University.

Figure 3-5 A depicts representative IR spectra obtained as a function of position (at approximately equally spaced intervals) along a gradient film. The small, sharp peak at 1275 cm^{-1} is due to a $Si-CH_3$ deformation mode[88] and is diagnostic for film methyl content. The methyl C-H stretching band near 2900 cm^{-1} could not be employed because of overlap with the absorption of unhydrolyzed methoxy groups present in some film regions. The 1275 cm^{-1} peak shows a gradual increase in intensity along the gradient, as expected for a film of gradually

increasing methyl content. A broad absorption band around 3400 cm^{-1} was also found in the spectra, consistent with the presence of some residual water in the films.

As a means to compensate for the aforementioned film thickness variations, the ratio of the Si-CH_3 (1275 cm^{-1}) and Si-O-Si (1080 cm^{-1}) peak heights was also calculated and used to follow film methyl content. Figure 3-5B plots these data. Shown are average peak height ratios (and their standard deviations) obtained from three spectra recorded at each point (±150 μm) along the gradient. As expected, the Si-CH_3/Si-O-Si peak ratio increases from the top of the gradient (0 mm) to the bottom (16 mm). The IR data suggest a linear dependence of methyl content on gradient position, though such a simple dependence is not generally expected.[87] Nevertheless, the observed change in Si-CH_3/Si-O-Si peak ratio suggests a five-fold increase in film methyl content along the measured range of the gradient. Measurements of the 3400 cm^{-1} peak height relative to the Si-O-Si peak showed no detectable trend (at the 90% confidence level) in water content along the gradient.

3.2.3 Fluorescence imaging

Figures 3-6 A,C depict representative frames (~44 μm x 44 μm) from fluorescence videos acquired near the top (2 mm from the start) of a dye-doped gradient and near the bottom (12 mm), respectively. These particular videos were acquired at 1 frame per second (1 fps) using incident laser intensities of ~50 W/cm^2. Videos were also acquired at faster frame rates (up to 3 fps) and higher and lower intensities, but the former were determined to produce videos of highest signal-to-noise, while avoiding excessive photobleaching of the dye.

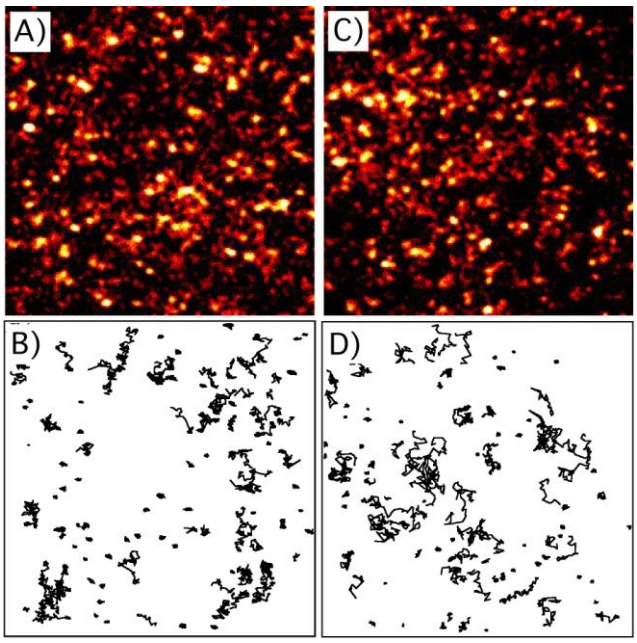

Figure 3-6. A) and B) Representative video frame and single molecule trajectories, respectively, obtained from a widefield video recorded near the top (2 mm) of a silica film gradient. C) and D) Representative video frame and trajectories, respectively, obtained from a widefield video recorded near the bottom (12 mm) of the same gradient.

Individual fluorescent spots in each video frame were detected and linked into trajectories depicting the frame-to-frame motions of the individual molecules. The goal was to use these trajectories to determine single molecule diffusion coefficients and to explore film nanostructure. Therefore, a relatively high concentration of dye was employed (see Figures 3-6 A,C). The high dye concentration precluded manual tracking and linking of the fluorescent spots. Instead, a modified plug-in for the ImageJ software was employed to generate an initial set of trajectories.[89] Automated particle detection and tracking was only applied to the final 350 frames of each video, in order to avoid linking errors caused by the higher dye concentration (prior to modest photobleaching) observed in the initial video frames. A two-point smooth was applied to each frame to increase signal-to-noise and aid in particle detection and tracking. The full set of trajectories generated was subsequently truncated to include only those ≥20 frames in length. These trajectories were then manually inspected and, when necessary, adjusted to correct residual linking errors and to separate trajectory segments exhibiting clear changes in behavior (i.e., switching from fixed to mobile behavior). Statistical tests were employed to ensure the errors and/or changes in behavior observed were significant, prior to making any changes to

individual trajectories. For fixed molecules, linking errors were only corrected if the questionable point fell at a distance > 4s (s representing the standard deviation) from the mean position of the spot in the remainder of the frames. For molecules exhibiting a change in behavior, the appropriate Student's t-test was applied to determine, for example, whether the apparent diffusion coefficient was statistically different before and after the apparent change, at the 95% confidence level.

As is apparent from the data plotted in Figure 3-6, these particular film regions incorporate at least two distinct populations of molecules: one in which the molecules are adsorbed to or otherwise entrapped at fixed locations in or on the films, and a second in which the molecules are relatively mobile, wandering over many square microns during the recording of a single video. With the exception of videos recorded at the very top of the gradient (0 mm), all videos recorded along the gradient films depict the presence of these two populations.

At the top of the gradient (0 mm), virtually all molecules detected were found to remain in fixed locations. Control experiments performed with dye loaded in spin-coated TMOS sublayers in the absence of a gradient overlayer exhibited behavior indistinguishable from that observed at the top of the gradient: virtually all molecules were found to be immobile. This observation is consistent with those of a number of previous single molecule studies in which spin-coated, dye-doped TMOS-derived films incorporated predominantly immobile molecules.[49,90,91] In contrast, dye loaded TMOS films prepared by dip coating were found to incorporate significant populations of mobile molecules, as observed in the gradient samples. It is therefore concluded that the dye found at the 0 mm position is adsorbed in/on the TMOS sublayer. It is further concluded that this position falls just above the start of the actual gradient (corresponding to the rough region observed by ellipsometry) and that the dye likely migrated there during dip coating or film drying. Note that it was only possible to determine the start of each gradient to within ±1 mm on the glass substrates. While data at the 0 mm position is shown below for completeness, it is not included in any of the discussion or conclusions.

3.2.3 Evolution of diffusion coefficients.

Diffusion coefficients were obtained from the individual trajectories by calculating the mean square displacement (MSD) of each molecule in time.[58,92] For a free random walk in two dimensions, the MSD increases linearly as 4Dt, where D is the diffusion coefficient and t is time.

In the present studies, the video frame time was 1.03 s. Many of the MSD vs time plots obtained were found to remain linear only over short times (i.e. < 15 s), while on longer time scales, significant deviations from linearity were often observed. Saxton has demonstrated that such deviations from linearity can arise from random variations in the trajectories that mimic the effects of anomalous sub- and super-diffusion, even in homogeneous materials.[93] Simulations of homogeneous samples suggest this is the case here. Therefore, only short-time diffusion coefficients[58] were employed in the present analysis. These were obtained from each trajectory by determining the slope of the MSD plots (see Figure 3-7) across only the first three data points (i.e., for t = 1, 2, 3 s). Figure 3-7 (left column) depicts histograms of the D values obtained, as a function of position along a single gradient. The data shown were acquired after drying the gradient for 5 d in a dessicator.

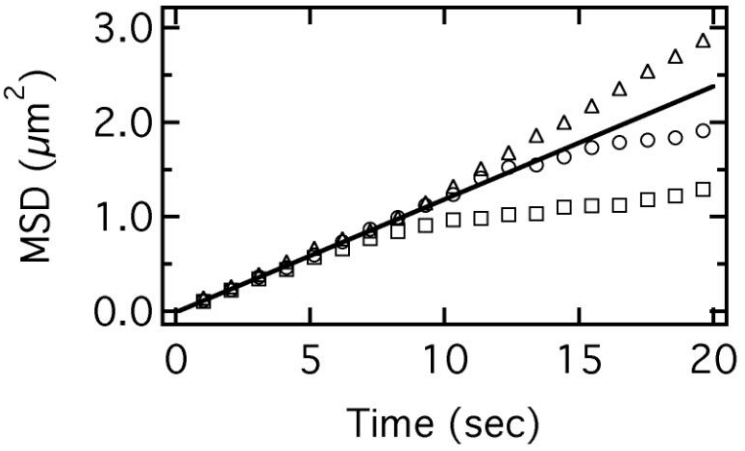

Figure 3-7. Representative single trajectory MSD plots showing deviation from expected linearity at relatively long times. Diffusion coefficients were obtained from individual MSD plots like these by determining the slope of each plot across the first three data points. The trajectories shown were ≥ 40 frames long. The different symbols depict data from three different trajectories obtained from a single video near the middle of the gradient (6 mm).

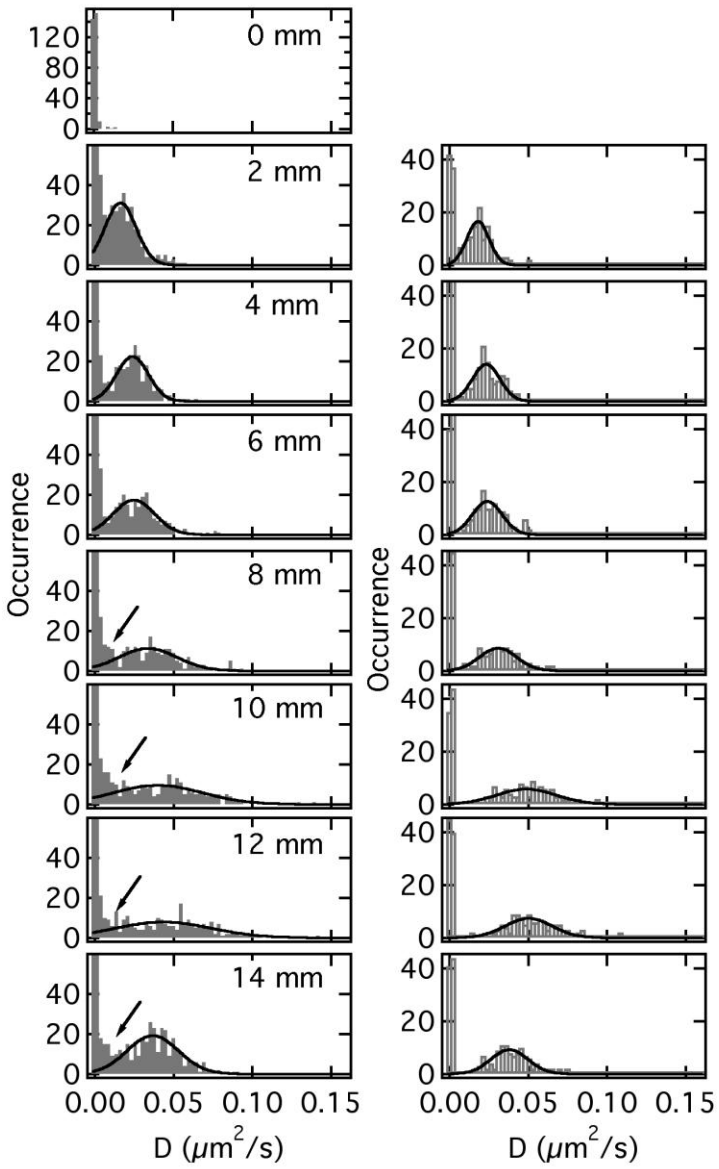

Figure 3-8. Left) Histograms showing D values obtained from several hundred trajectories recorded at each point along a five-day dried silica film gradient. These data depict the presence of fixed (D ~ 0) and mobile populations. The solid curves depict Gaussian fits of the most rapidly moving population of mobile molecules. The arrows point to a second, minority population of less mobile molecules found in some regions. Right) Histograms showing D values from simulated videos incorporating distinct populations of fixed and mobile molecules, the latter having D values similar to those of the experimental data (Left). The y-scales in all but the 0 mm plot have been expanded to better show the mobile populations, truncating the immobile populations.

As mentioned above, regions that fall within the gradient (i.e., 2 mm – 14 mm) incorporate both an immobile population (D ~ 0) and a mobile population (D > 0). The majority of mobile molecules at each point along the gradient yield D values that fall within a single Gaussian distribution, as shown in Figures 3-8. The mean D values obtained from the fitted mobile populations are plotted in Figure 3-9A. A monotonic trend towards larger D values is observed between the TMOS (2 mm) and MTMOS (12 mm) ends of the gradient, indicative of an increase in molecular mobility as the methyl content of the film increases. The decrease in D observed at 14 mm is likely due to imperfections in the film at the bottom of the gradient and/or increased interaction of the dye with the sublayer, due to thinning of the film.

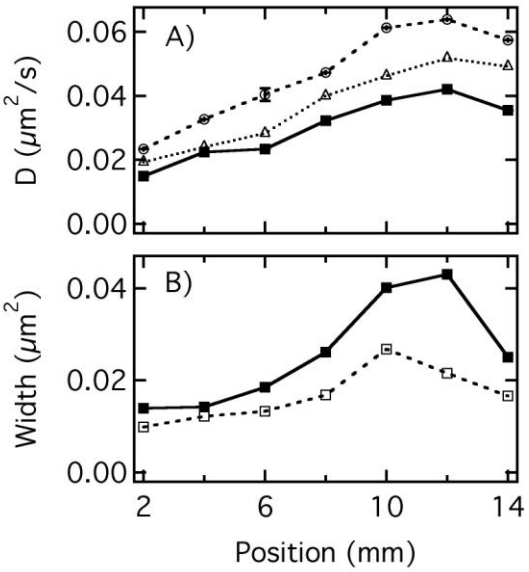

Figure 3-9. A) Mean D values obtained from the Gaussian fits to the experimental data shown in Figure 3-8 for the five-day dried gradient (filled squares) and corresponding data for the three-day dried (open triangles) and one-day dried (open circles) gradient. B) Width of the Gaussian fits to the mobile fraction of molecules along the five-day dried gradient (filled squares) and for the simulated data (open squares). The experimental data exhibit broader distributions, suggestive of modest heterogeneity, particularly at the MTMOS end of the gradient.

The data shown in Figure 3-9A also depict a trend towards smaller D values as the films dry. The slow evolution of sol-gel-derived silica materials properties is a well-known phenomenon that has been extensively studied in the past for non-gradient materials.[15,94-96]

Generally, these temporal variations are a result of continued cross-linking and densification of the matrix, along with evaporation of residual solvent. Unless otherwise noted, the discussion presented below is restricted to data obtained from the 5 d dried sample. Longer drying periods were avoided due to concerns over contamination by fluorescent species.

Although the data reported here are derived from a single gradient sample, these same experiments were performed on several different gradients. All exhibited clear trends toward greater molecular mobility at the MTMOS end of the gradient and a gradual decline in mobility as the films dried. The D values obtained at similar positions along the replicate gradients, however, were found to vary significantly (i.e., by a factor of four or more). These variations are attributable to changes in the ambient laboratory temperature and humidity during sol and film preparation and aging, but may also result from variations in the degree of sol mixing during dip coating. As a result, it is only possible to draw quantitative comparisons between data obtained at different times and from different regions of the same film.

As noted above, all gradient regions incorporated a significant population of immobile molecules. This population was found to be invariant along the gradient, yielding an average of 288(±22) immobile molecules in the 44 μm x 44 μm areas imaged, as determined by summing the number of trajectories in the first two bins of each histogram shown in Figure 3-8. As virtually all molecules found on TMOS-sublayer coated substrates (see above) were found to be immobile, and significant populations of mobile molecules were found in non-gradient dip-coated TMOS and MTMOS films, it is concluded that the immobile population is dominated by Nile Red molecules entrapped in/on the TMOS sublayer.

In contrast to the immobile population, the number of mobile molecules (i.e. those not counted as immobile) varied in a non-monotonic manner, with relatively larger populations at either end (~ 350 molecules, excluding 0 mm) of the gradient and somewhat smaller ones in middle (~260). The spatial variations in the number of mobile molecules are attributed collectively to competition between film thinning, increased Nile Red solubility in methyl-modified gradient regions, and an increase in Nile Red fluorescence quantum yield[97,98] in these same regions.

The observed increase in Nile Red mobility (i.e., increasing D) running down the gradient has several possible origins. First, as MTMOS and TMOS have three and four hydrolyzable groups, respectively, the MTMOS end of the gradient is expected to be less dense, with reduced

cross-linking between the silica particles comprising the film. Likewise, these same structural differences suggest a reduction in the concentration of silanol (Si-OH) species towards the MTMOS end of the gradient. Silanol species can serve as hydrogen bonding sites for Nile Red,[90] slowing molecular diffusion at the TMOS end. Third, sol-gel materials derived from organosilane precursors can form viscous liquid-like oligomers,[49] thus providing a matrix that supports molecular diffusion. At the present time, no conclusions can be drawn as to the exact chemical/physical origins of the increase in molecular mobility as a function of position along the gradient. Regardless, all possibilities mentioned above are a consequence of increasing methyl content along the gradient. It should be noted that residual water found in the film could also facilitate molecular diffusion. However, increased molecular mobility at the MTMOS end would suggest increased water content in this region. Higher water content at the MTMOS end is neither expected (the MTMOS end is more hydrophobic)[87] nor observed by ellipsometry and IR imaging. The exact origins of the spatial variations in mobility will be the subject of future publications.

3.2.5 Gradient structure and heterogeneity.

As shown previously by our group[90,91,99,100] and others,[101] sols prepared by mixing separately hydrolyzed precursors often form heterogeneous films incorporating "phase separated" domains of the individual sol components. Characterization of these materials was accomplished previously by atomic force microscopy[99,101] (e.g., tapping mode phase imaging) and by IR,[100] bright field optical and fluorescence microscopies.[101] While these studies provided valuable information on certain film properties, the single molecule data reported here provide complementary results that allow for assessment of the role played by materials heterogeneity in governing molecular mobility.

The degree to which materials heterogeneity contributes to the widths of the experimentally-determined D distributions depicted in Figure 3-8 was assessed by comparing these data to those from simulated videos. The simulations were done by Dr. Higgins (KSU Chemistry). Briefly, individual molecules were positioned randomly across each simulated region. A minority (40%) of the molecules were assigned to fixed locations, while the remainder moved about the region by free (unconfined) Brownian motion. The simulations were run using a range of diffusion coefficients to mimic the positional variations in D along the gradients.

However, all mobile molecules in individual simulations were assigned identical D values. Each simulated molecule was also assigned a random lifetime determined from an exponential distribution having a mean of 15 s. Diffusion coefficients were obtained from the simulated data in a manner identical to those obtained from experimental data. Notably, as the simulated data also produced MSD plots that deviated from linearity on long times (see Figure 3-7), D values were again calculated only from the MSD plot slopes at short times. As shown in Figure 3-8 and 3-9 B, the D value distributions obtained from the simulated and experimental data have similar widths that generally increase with increasing D. Interestingly, the distribution widths are more similar near the top of the gradient, and differ more significantly near the bottom. The experimental distributions are 32% wider, on average, than the simulated distributions for the first three points along the gradient. The remainder of the experimental data produce distributions 64% wider than the simulated results. In general, these observations indicate that the diffusion coefficients for the majority of mobile molecules are only modestly more variable than expected for free diffusion in a perfectly homogeneous film. However, the variability in D is clearly greater in regions of high methyl content, suggesting increased heterogeneity towards the bottom of the gradient.

Spatial variations in film heterogeneity are also reflected in the observation of a second, minority population of mobile molecules that appears in the experimental data towards the bottom of the gradient. This population is highlighted by the arrows appended to Figure 3-8 and is distinctly less mobile than the majority. Visual inspection of the associated trajectories indicates that their appearance does not arise from spot tracking or linking errors. The absence of such molecules in the simulated data provides additional support for this conclusion. Their presence is also not due to the increased occurrence of molecules that switch between diffusing and adsorbed/entrapped states, as the few trajectories exhibiting such behavior were purposefully separated into fixed and mobile segments (see above). It is concluded that this second, less mobile population is due to the presence of film domains in which the molecules are less mobile. These domains may be rich in TMOS and may be dispersed among MTMOS rich regions. The exact size of these domains is unknown at present, but must be larger than $4D\tau$, where τ is the total time of observation. Using nominal values for D and τ of 0.01 $\mu m^2/s$ and 20 s, respectively, the domains are estimated to be > 0.8 μm^2 in size.

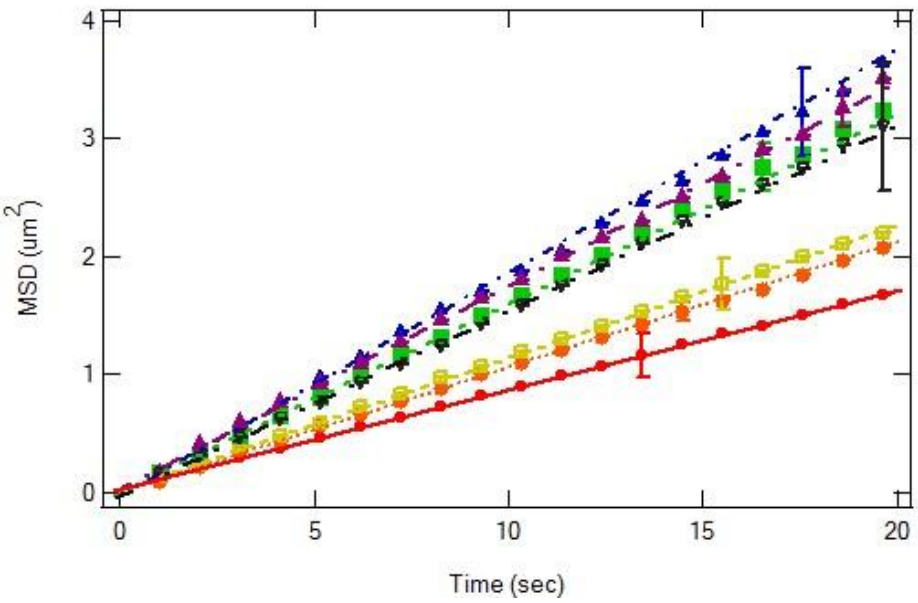

Figure 3-10. MSD as a function of time, averaged over all mobile molecules (individual trajectories with frame-to-frame MSD > 0.05 μm^2) as a function of position along a five day dried silica film gradient. The standard deviations are obtained from all MSD value of each position. The Data are shown for 2 mm (open circles), 4 mm (filled circles), 6 mm (open squares), 8 mm (filled squares), 10 mm (open triangles), 12 mm (filled triangles) and 14 mm (open inverted triangles) positions. The solid lines depict fits of the MSD values to a line during the first 5 s of data. The linear increase in MSD with time in each case provides important evidence of free diffusion within the gradient films.

Further information on the nature of film heterogeneity in the gradient, and its influence on molecular diffusion was obtained from plots of average MSD vs time for the main population of mobile molecules. The less mobile population was deemed too small to extract from the nearby immobile population to be useful in such calculations. As noted above, MSD for molecules exhibiting free diffusion in two dimensions should increase linearly in time. Figure 3-10 plots these data for each position along the five-day dried sample. Here, *average* MSD data is plotted from trajectories ≥ 40 frames in length. While single trajectory MSD data (see Figure 3-7) could potentially provide better information on local variations in film properties, as noted above, such plots are often biased by random trajectory fluctuations that mimic anomalous sub- and super-diffusion, especially for trajectories of relatively short lengths.[93] As is readily apparent from the data shown in Figure 3-10, the average MSD increases linearly in time for all points along the gradient. This observation provides strong evidence that diffusion of the probe

dye molecules is free (i.e., unhindered) along the full length of the gradient. While the present gradient exhibits (as do replicate samples) clear evidence for at least two populations of mobile molecules, the data shows no evidence that the Nile Red molecules are restricted to the associated film domains. It is concluded that the dye molecules pass freely between these regions.

Chapter 4 - Conclusion and Future Work

Silica thin films incorporating polarity gradients have been prepared by using an "infusion-withdrawal dip-coating" procedure. Results from fluorescence spectroscopy and contact angle measurements provide evidence that the films obtained incorporate polarity gradients derived from increasing concentrations of methyl-modified silica. Single molecule tracking data obtained from Nile Red doped gradient films depict the presence of immobile molecules entrapped in the silica sublayer and two distinct populations of mobile molecules within the gradient overlayer. The mobility of the latter populations was observed to increase as the methyl content of the film increased down the gradient, which has several possible origins. First, the MTMOS end of the gradient is expected to be less dense with reduced cross-linking between the silica particles comprising the film, as MTMOS and TMOS have three and four hydrolyzable groups, respectively. Second, these same structural differences sugest a reduction in the concentration of silanol species towards the MTMOS end of the gradient. Silanol species can serve as hydrogen bonding sites for Nile Red, slowing molecular diffusion at the TMOS end. Third, sol-gel materials drived from organosilane precusors can form viscous liquid-like oligomers, thus providing a matrix that supports molecular diffusion. At the present time, no conclusions can be drawn as the exact chemical/physical origins of the increasing molecular mobility as a function of position along the gradient. The distribution in D values obtained from the majority population of mobile molecules was found to be only modestly broader than expected for free 2D diffusion in a homogeneous matrix. However, the presence of the second, minority population of less mobile molecules was concluded to reflect micron-scale heterogeneity in the films, likely arising from the formation of phase separated domains of TMOS and MTMOS-rich materials.[99,101] The dye molecules were, however, concluded to pass freely between these domains, as suggested by a lack of evidence for confined diffusion in all gradient regions.

The above-mentioned single molecule study has given proof of interactions between single molecules and their local chemical environment. It is important to know how the dye molecules partition between silica films for the potential applications of such materials (chemical separation, catalysts and sensors). Future studies of silica thin film gradients will include

investigations of such heterogeneity by implementation of atomic force and single molecule microscopy methods. A few additional experiments might be achieved based on the research described in this thesis. In addition, since we have prepared good and uniform silica thin films with polarity gradients, other gradients might also be achieved by using the same or similar "infusion withdrawal dip-coating" methods.

References

(1) Ye, F.; Cui, C.; Kirkeminde, A.; Dong, D.; Collinson, M. M.; Higgins, D. A. *Chem. Mater* **2010**, *22*, 2970-2977.

(2) Avnir, D. *Acc. Chem. Res.* **1995**, *28*, 328-334.

(3) Collinson, M. M. *Trends in Anal. Chem.* **2002**, *21*, 30-38.

(4) Walcarius, A.; Mandler, D.; Cox, J. A.; Collinson, M. M.; Lev, O. *J. Mater. Chem.* **2005**, *15*, 3663-3689.

(5) Dunn, B.; Zink, J. I. *Acc. Chem. Res.* **2007**, *40*, 747-755.

(6) Holthoff, E. L.; Bright, F. V. *Acc. Chem. Res.* **2007**, *40*, 756-767.

(7) Brennan, J. D. *Acc. Chem. Res.* **2007**, *40*, 827-835.

(8) Walcarius, A.; Collinson, M. M. *Annu. Rev. Anal. Chem.* **2009**, *2*, 121-143.

(9) Liedberg, B.; Tengvall, P. *Langmuir* **1995**, *11*, 3821-3827.

(10) Senkan, S. *Angew. Chem., Int. Ed* **2001**, *40*, 312-319.

(11) Cabrera, C. R.; Finlayson, B.; Yager, P. *Anal. Chem.* **200**, *73*, 658-666.

(12) Wei, H.; Collinson, M. M. *Anal. Chim. Acta* **1999**, *397*, 113-121.

(13) Skrdla, P. J.; Mendes, S. B.; Armstrong, N. R.; Saavedra, S. S. *J. Sol-Gel Sci. Tech.* **2002**, *24*, 167-173.

(14) Marxer, S. M.; Schoenfisch, M. H. *Anal. Chem.* **2005**, *77*, 848-853.

(15) Tang, Y.; Tehan, E. C.; Tao, Z.; Bright, F. V. *Anal. Chem.* **2003**, *75*, 2407-2413.

(16) Sandee, A. J.; Reek, J. N. H.; Kamer, P. C. J.; van Leeuwen, P. W. N. M. *J. Am. Chem. Soc.* **2001**, *123*, 8468-8476.

(17) Gelman, F.; Blum, J.; Avnir, D. *New J. Chem.* **2003**, *27*, 205-207.

(18) Rodriguez, S. A.; Colon, L. A. *Chem. Mater.* **1999**, *11*, 754-762.

(19) Hayes, J. D.; Malik, A. *Anal. Chem.* **2000**, *72*, 4090-4099.

(20) Roux, R.; Puy, G.; Demesmay, C.; Rocca, J.-L. *J. Sep. Sci.* **2007**, *30*, 3035-3042.

(21) Brinker, C. J.; Scherer, G. W. *Sol-Gel Science: The Physics and Chemistry of Sol-Gel Processing*; Academic Press: Boston, 1990.

(22) Collinson, M. M. *Academic Press: New York* **2001**, *5*, 163-194.

(23) Schmidt, H. *J. Sol-Gel Sci. Tech.* **1994**, *1*, 217-231.

(24) Wen, J.; Wilkes, G. L. *Chem. Mater.* **1996**, *8*, 1667-1681.

(25) Genzer, J.; Bhat, R. R. *Langmuir* **2008**, *24*, 2294-2317.

(26) Morgenthaler, S.; Zink, C.; Spencer, N. D. *Soft Matter* **2008**, *4*, 419-434.

(27) Thami, T.; Bresson, B.; Fretigny, C. *J. Appl. Polym. Sci.* **2007**, *104*, 1504-1516.

(28) Elwing, H.; Welin, S.; Askendal, A.; Nilsson, U.; Lundstrom, I. *J. Colloid Interface Sci.* **1987**, *119*, 203-210.

(29) Golander, C. G.; Caldwell, K.; Lin, Y.-S. *Colloids and Surfaces* **1989**, *42*, 165-172.

(30) Chaudhury, M. K.; Whitesides, G. M. *Science* **1992**, *256*, 1539-1541.

(31) Lin, Y. S.; Hlady, V. *Colloids and Surfaces B: Biointerfaces* **1995**, *4*, 65-75.

(32) Daniel, S.; Chaudhury, M. K. *Langmuir* **2002**, *18*, 3404-3407.

(33) Choi, S.-H.; Newby, B. Z. *Langmuir* **2003**, *19*, 7427-7435.

(34) Genzer, J.; Efimenko, K.; Fischer, D. A. *Langmuir* **2006**, *22*, 8532-8541.

(35) Lobnik, A.; Wolfbeis, O. S. *Journal of Sol-Gel Science and Technology* **2001**, *20*, 303-311.
(36) Keeling-Tucker, T.; Brennan, J. D. *Chem. Mater* **2001**, *13*, 3331-3350.
(37) Zou, H.; Wu, S.; Shen, J. *Chem. Rev.* **2008**, *108*, 3893-3937.
(38) Dunn, B.; Zink, J. I. *Chem. Mater* **1997**, *9*, 2280-2291.
(39) Kanungo, M.; Collinson, M. M. *Langmuir* **2005**, *21*, 827-829.
(40) Collinson, M. M. *Acc. Chem. Res.* **2007**, *40*, 777-783.
(41) Collinson, M. M.; Howells, A. R. *Anal. Chem.* **2000**, *72*, 702-709.
(42) Lev, O.; Wu, Z.; Bharathi, S.; Glezer, V.; Modestov, A.; Gun, J.; Rabinovich, L.; Sampath, S. *Chem. Mater* **1997**, *9*, 2354-2373.
(43) Privett, B. J.; Shin, J. H.; Schoenfisch, M. H. *Anal. Chem.* **2010**, *82*, 4723-4742.
(44) Balss, K. M.; Coleman, B. D.; Lansford, C. H.; Haasch, R., T.; Bohn, P. W. *J. phys. Chem. B* **2001**, *105*, 8970-8979.
(45) May, E. L.; Hillier, A. C. *Anal. Chem.* **2005**, *77*, 6487-6495.
(46) Plummer, S. T.; Bohn, P. W. *Langmuir* **2002**, *28*, 4142-4149.
(47) Terrill, R. H.; Balss, K. M.; zhang, Y.; Bohn, P. W. *J. Am. Chem. Soc.* **2000**, *122*, 988-989.
(48) Higgins, D. A.; Collinson, M. M.; Saroja, G.; Bardo, A. M. *Chem. Mater.* **2002**, *14*, 3734-3744.
(49) Martin-Brown, S. A.; Fu, Y.; Saroja, G.; Collinson, M. M.; Higgins, D. A. *Anal. Chem.* **2005**, *77*, 486-494.
(50) Ye, F.; Collinson, M. M.; Higgins, D. A. *Phys. Chei. Chem. Phys.* **2009**, *11*, 66-82.
(51) Ye, F.; Higgins, D. A.; Collinson, M. M. *J. Phys. Chem. C* **2007**, *111*, 8.
(52) Fu, Y.; Ye, F.; Sanders, W. G.; Collinson, M. M.; Higgins, D. A. *J. Phys. Chem. B,* **2006**, 6772-6778.
(53) Striova, J.; Higgins, D. A.; Collinson, M. M. *Langmuir* **2005**, *21*, 6137-6141.
(54) Higgins, D. A.; Collinson, M. M. *Langmuir Invited Feature Article* **2005**, *21*, 9023-9031.
(55) Orrit, M.; Bernard, J. *Phys. Rev. Lett.* **1990**, *65*, 2716-2719.
(56) Schmidt, T.; Schu¨tz, G. J.; Baumgartner, W.; Gruber, H. J.; Schindler, H. *Biophysics* **1996**, *93*, 2926-2929.
(57) Elson, E.; Magde, D. *Biopolymers* **1974**, *13*, 1-28.
(58) McCain, K. S.; Hanley, D. C.; Harris, J. M. *Anal. Chem.* **2003**, *75*, 4351-4359.
(59) Moerner, W. E.; Fromm, D. P. *REVIEW OF SCIENTIFIC INSTRUMENTS* **2003**, *74*, 3597-3620.
(60) Schmide, T.; Schutz, G. J.; barumgertner, W.; Gruber, H. J.; Shinder, H. *Proc. Natl. Acad. Sci. USA* **1996**, *93*, 2926-2929.
(61) Collinson, M. M.; Zambrano, P. J.; Wang, H.; Taussig, J. S. *Langmuir* **1999**, *15*, 662-668.
(62) Howells, A. R.; Zambrano, P. J.; Collinson, M. M. *Analytical Chemistry* **2000**, *72*, 5265-5271.
(63) Hanley, D. C.; Hanley, D. C. *Analytical Chemistry* **2001**, *73*, 5030-5037.
(64) Hansen, R. L.; Harris, J. M. *Analytical Chemistry* **1998**, *70*, 2565-2575.
(65) Striova, J.; Higgins, D. A.; Collinson, M. M. *Langmuir* **2005**, *21*, 6137-6141.

(66) Wetzel, D. L.; Striovab, J.; Higgins, D. A.; Collinson, M. M. *Vibrational Spectroscopy* **2004**, *35*, 153-`58.
(67) Higgins, D. A.; Collinson, M. M.; Saroja, G.; Bardo, A. M. *Chem. Mater.* **2002**, *14*, 3734-3744
(68) Goring, G. L. G.; Brennan, J. D. *Chem. Mater* **2007**, *19*, 5336-5346.
(69) Langereis, E.; Heil, S. B. S.; Knoops, H. C. M.; Keuning, W.; Van de Sanden, M. C. M.; Kessels, W. M. M. *Journal of Physics D: Applied Physics* **2009**, *42*, 73001-73020.
(70) Aulika, I.; Dejneka, A.; Zauls, V.; Kundzins, K. *J. Electrochem. Soc.* **2008**, *155*, G209-211.
(71) Brinker, C. J.; Frye, G. C.; Hurd, A. J.; Ashley, C. S. *Thin Solid Films* **1991**, *201*, 97-108.
(72) Nishida, F.; McKiernan, J. M.; Dunn, B.; Zink, J. I.; Brinker, C. J.; Hurd, A. J. *Journal of the American Ceramic Society* **1995**, *78*, 1640-1648.
(73) Chaudhury, M. K.; Whitesides, G. M.; *Science* **1992**, *256*, 1539-1541.
(74) Ueda-Yukoshi, T.; Matsuda, T. *Langmuir* **1995**, *11*, 4135-4140.
(75) Morgenthaler, S.; Lee, S.; Zuercher, S.; Spencer, N. D. *Langmuir* **2003**, *19*, 10459-10461.
(76) Yu, X.; Wang, Z.; Jiang, Y.; Zhang, X. *Langmuir* **2006**, *22*, 4483-4486.
(77) Park, H. Y.; Kang, D. P.; Na, M. K.; Lee, H. W.; Lee, H. H.; Shin, D. S. *Journal of Electroceramics* **2009**, *22*, 309-314.
(78) Jitianu, A.; Amatucci, G.; Klein, L. C. *Journal of Materials Research* **2008**, *23*, 2084-2090.
(79) Monde, T.; Fukube, H.; Nemoto, F.; Yoko, T.; Konakahara, T. *Journal of Non-Crystalline Solids* **1999**, *246*, 54-64.
(80) Bhagat, S. D.; Oh, C.-S.; Kim, Y.-H.; Ahn, Y.-S.; Yeo, J.-G. *Microporous and Mesoporous Materials* **2007**, *100*, 350-355.
(81) Rao, A. V.; Kulkarni, M. M.; Amalnerkar, D. P.; Seth, T. *Journal of Non-Crystalline Solids* **2003**, *330*, 187-195.
(82) Quere, D. *Physica A: Statistical Mechanics and Its Applications (Amsterdam, Netherlands)* **2002**, *313*, 32-46.
(83) Chau, T. T.; Bruckard, W. J.; Koh, P. T. L.; Nguyen, A. V. *Advances in Colloid and Interface Science* **2009**, *150*, 106-115.
(84) Deye, J. F.; Berger, T. A.; Anderson, A. G. *Analytical Chemistry* **1990**, *62*, 615-622.
(85) Hou, Y.; Bardo, A. M.; Martinez, C.; Higgins, D. A. *Journal of Physical Chemistry B* **2000**, *104*, 212-219.
(86) Bardo, A. M.; Collinson, M. M.; Higgins, D. A. *Chem. Mate.* **2001**, *13*, 2713-2721.
(87) Ye, F.; Cui, C.; Kirkeminde, A.; Dong, D.; Collinson, M. M.; Higgins, D. A. *Chem. Mater* **2010**, *22*, 2970-2977.
(88) Kim, S.; Toivola, Y.; Cook, R. F.; Char, K.; Chu, S.-H.; Lee, J.-K.; Yoon, D. Y.; Rhee, H.-W. *J. Electrochem. Soc.* **2004**, *151*, F37-F44.
(89) Levy, G., Particle Tracher. http://rsb.info.nih.gov/ig/ 2009
(90) Bardo, A. M.; Collinson, M. M.; Higgins, D. A. *Chem. Mater.* **2001**, *13*, 2713-2721.

(91) Higgins, D. A.; Collinson, M. M.; Saroja, G.; Bardo, A. M. *Chem. Mater.* **2002**, *14*, 3734-3744.
(92) Schmidt, T.; Schutz, G. J.; Baumgartner, W.; Gruber, H. J.; Schindler, H. *Proc. Natl. Acad. Sci.* **1996**, *93*, 2926-2929.
(93) Saxton, M. J. *Biophys. J.* **1993**, *64*, 1766-1780.
(94) Narang, U.; Wang, R.; Prasad, P. N.; Bright, F. V. *J. Phys. Chem.* **1994**, *98*, 17-22.
(95) Howells, A. R.; Zambrano, P. J.; Collinson, M. M. *Anal. Chem.* **2000**, *72*, 5265-5271.
(96) Dunbar, R. A.; Jordan, J. D.; Bright, F. V. *Anal. Chem.* **1996**, *68*, 604-610.
(97) Sarkar, N.; Das, K.; Nath, D. N.; Bhattacharyya, K. *Langmuir* **1994**, *10*, 326-329.
(98) Dutta, A. K.; Kamada, K.; Ohta, K. *J. Photochem. Photobiol. A* **1996**, *93*, 57-64.
(99) Striova, J.; Higgins, D. A.; Collinson, M. M. *Langmuir* **2005**, *21*, 6137-6141.
(100) Wetzel, D. L.; Striova, J.; Higgins, D. A.; Collinson, M. M. *Vib. Spectrosc.* **2004**, *35*, 153-158.
(101) Goring, G. L. G.; Brennan, J. D. *Chem. Mater* **2007**, *19*, 5336-5346.